Alfred Wegener Institute
Helmholtz Centre for Polar and Marine Research

and

Free University of Berlin
Department of Earth Sciences
Institute of Meteorology

Simulated climate and vegetation patterns during the Pliocene using an Earth System Model

Bachelor thesis

Stephanie Meier (5015873)
B. Sc. Meteorology

Submitted: 15.08.2019

Reviewer:
Prof. Dr. Gerrit Lohmann (Alfred Wegener Institute)
and
Dr. Ingo Kirchner (Free University of Berlin)

Abstract

Die Zeitperiode des mittleren Pliozäns (vor ca. 3.264 bis 3.025 Ma) bietet eine gute Grundlage für Sensitivitätsstudien mit einem erhöhten CO_2-Wert von 400 ppmv. Mit der Erde als komplexem System lässt sich insbesondere anhand von Modelldaten die Wechselwirkung verschiedener Teile des Klimasystems wie Atmosphäre, Ozean und Landoberfläche untersuchen, was im Rahmen des PlioMIP2 getan wird. Hier wird der Einfluss von Temperatur und Niederschlag auf die Ausbreitung verschiedener Pflanzentypen unter Anpassung des CO_2-Wertes und der Anpassung von Orographie und Eisschild mittels Modelldaten analysiert und mit dem Bestimmtheitsmass korreliert. Es tritt im pliozänen Hauptexperiment mit angepassten Randbedingungen wie 400 ppmv im Vergleich zu präindustriellen 280 ppmv Konfigurationen eine mittlere globale Erwärmung von 3.20°C auf mit einer Verschiebung der Minima und Maxima von -77 zu -67°C bzw. 43 auf 49°C. Dies, und auch die lokale Änderung des Niederschlags, bewirkt eine Verschiebung der Baumgrenze in Asien, Nordafrika und Nordamerika von bis zu 2200 km, begleitet durch einen Rückgang der Grasbedeckung. Letztere expandiert allerdings auf Kosten von Baumbedeckung im Amazonas-Regenwald und Europa. Lokale Untersuchungen von Sibirien und Sahelzone ergaben meist signifikante Korrelation zwischen den Änderungen der dort vorherrschenden Pflanzentypen und der Temperatur, nicht aber zwischen den Änderungen der Pflanzentypen und des Niederschlags.

The Mid-Pliocene Warm Period (ca. 3.264 to 3.025 Ma) provides a suitable test bed for sensitivity studies with enhanced CO_2 concentration of 400 ppmv. With the Earth being a complex system, especially model data allows analyses of the interaction of different subsystems of the Earth's climate, as done by the PlioMIP2. In this case the influence of temperature and precipitation on the growth of different plant types with adaptations in CO_2 concentration as well as orography and ice sheets is analysed, and correlation is tested with the coefficient of determination. In difference to the pre-industrial configuration with 280 ppmv, the mid-Pliocene experiment of 400 ppmv gives a global warming of 3.20°C with a shift of minima and maxima from -77 to -67°C and 43 to 49°C. This, in addition to regional changes in precipitation, leads to a northward shift of treeline in Asia, North Africa and North America of up to 2200 km accompanied by a decrease of grass cover. Those, however, expand in regions like the Amazonian rainforest and Europe. Local analyses of Siberia and the Sahel Zone reveal mostly significant correlation of changes in plants and temperature, but not of changes in vegetation and precipitation.

Contents

1 Introduction and motivation

To understand the future climate it is important to accurately simulate the past. With a rising concentration of CO_2 from around 280 ppmv (parts per million per volume) at the Pre-Industrial time period up to more than 410 ppmv in 2019 following the Keeling Curve (Beck (2008)), the impact on atmosphere, hydrosphere, lithosphere and biosphere needs to be assessed. The last period a similar concentration of 400 ppmv occured was in the Mid-Pliocene (ca. 3.264 to 3.025 Ma), in which the global surface air temperature was 1.8 to 3.6°C higher than in the Pre-Industrial time frame (Hill et al. (2014)). Therefore it is thought to be an example of a climate with a raise of temperature in a magnitude that is as high as predicted for the 21st century (Chandler (1997)). The geologically recent occurence provides good paleoenvironmental data acquisition (Hill et al. (2014)) and therefore verification of modelled results of that time period (Dowsett et al. (2011), Salzmann et al. (2009)).
As the time period of the Pliocene is an important example for future changes in climate the Pliocene Model Intercomparison Project (PlioMIP) was created (Haywood et al. (2011)). As the results of the project, which is currently in Phase 2, give information about the Pliocene atmosphere, ocean and the vegetation states (more information in chapter 3), global processes and quantities like ocean circulation, changes in sea levels, ice-albedo feedback, atmospheric circulation and the climate-vegetation-feedback can be examined. With a paleogeography quite similar to the present geography a comparison of Pliocene and modern climate is relatively easy (Salzmann et al., 2011).
By better understanding the distribution of vegetation in the Pliocene, today's vegetation changes, mostly triggered by a rising CO_2-concentration and higher temperatures as a result of a stronger greenhouse effect, may be explained. Recent studies show that the ongoing climate warming causes, for example, shifts of the boreal ecosystems, which are exposed to the greatest climatic changes worldwide (Epp et al., 2018). A better understanding of the vegetation distribution provides a potential reference for future boreal vegetation shifts.

2 State of research of Mid-Pliocene climate

As research by modelling the paleoclimate is important both for understanding the past and predicting the future, an emphasis was put on this branch of research in the last decades. According to Haywood et al. (2013) the Paleoclimate Modelling Intercomparison Project (PMIP) was founded in 1991 for an organised collaboration of different countries and institutions. The main aim of the project was to assess the climate models' abilities to simulate past climates. As a component of that project, a more Pliocene-specific subproject, the Pliocene Modelling Intercomparison Project (PlioMIP), was created. At the start of the research, the Phase 1, experiments were run with atmosphere-only climate models as well as with models where ocean and atmosphere are coupled. The vegetation was defined to be prescribed. The results were mainly focused on the temperature differences like surface air temperature and sea surface temperature, because one objective was to quantify the climate and earth system sensitivity in general through adapted CO_2 concentrations (Haywood et al., 2013). In the PlioMIP1 as best estimate concentration of 405 ppmv of carbon dioxide was used (Haywood et al., 2011), because of proxies suggesting a range between about 365 and 415 ppmv (Pagani et al., 2009).
In Phase 2 of the PlioMIP more emphasis was put on the vegetation changes by employing different dynamic vegetation models as part of, or coupled with, the atmosphere models. Following Salzmann et al. (2008) by using the BIOME4 vegetation model, which utilizes the climatology of the Hadley Centre Atmospheric Model Version 3 (HadAM3) coupled with the vegetation model TRIFFID, the modelled results fit the proxy conditions quite well. In first experiments the group working with the HadAM3 experienced an increase of tree cover in high latitudes and a northward shift of savanna and grassland in expense of African desert. In the published paper by Salzmann et al. (2011) the BIOME4 model simulations are described and the analysed results are divided into tropical and subtropical, temperate and warm-temperate as well as polar and subpolar vegetation zones. In summary, the polar and subpolar zone show very prominent differences in the Arctic region, quite similar to the proxies found there. In difference to the Arctic, there are not many paleobotanical records for Antarctica, so a validation of the modelled results is more difficult and has not been done in total yet (Salzmann et al., 2011). The distribution of biomes with the HadAM3 and BIOME4 models is part of the analysis by Haywood et al. (2002), where a reconstruction with 73 terrestrial localities is employed. Their findings include four trends: Firstly there was is an increase of tundra

in high latitudes; secondly more evergreen taiga develops in expense of deciduous taiga; thirdly, tropical shrubland replaces deserts in low-latitudes; and last, overall, there are more forested areas, which are linked to an increase of precipitation. Latest research realized by the data assembled in PlioMIP Phase 2 was mainly focused on insulation effects on the Arctic amplification (Zheng et al., 2019), climate sensitivity (Chandan and Peltier, 2018) and Pliocene climate and warming (Chandan and Peltier (2017), Kamae et al. (2016)).
Overall, even though there are specialised studies carried out considering changes in Pliocene vegetation, there is still no analysis of the output of the Jena Scheme for Biosphere-Atmosphere Interaction in Hamburg (JSBACH) dynamic vegetation module for the PlioMIP2. The Alfred Wegener Institute (AWI) contribution to the PlioMIP by precparing and run experiments with the COSMOS model, which includes the JSBACH module (see Chapter 3). The AWI is the only member of the project using this specific climate model. Since there were no published results for this model in terms of PlioMIP2 no analysis of this simulation output das been performed in detail, yet.

3 Model

3.1 Data available in the PlioMIP2 Project

As part of the PlioMIP2-Project an ensemble of simulations with coupled ocean-atmosphere general circulation models (GCMs) has been performed. The experiments presented in this thesis are produced by the Department for Climate Science, Paleoclimate Dynamics of the AWI with the Community Earth System Models (COSMOS), which is later briefly described in chapter 3.2. The naming of the different simulations indicates the adjustments made to Pre-Industrial (PI) boundary conditions towards representation of the Pliocene as outlined below.
Following the paper published by Haywood et al. (2016) experiments named with solely 'E' are experiments based on modern orography, bathymetry and land-sea-mask, including soil and topography conditions. The ice sheets of Greenland as well as Antarctica are also kept as in modern day conditions.
A simulation named with 'Eo' indicates an experiment with PI ice sheet distribution but remaining geography as for Pliocene with a closed Bering Strait, closed Canadian Arctic Archipelago, as well as a closed Hudson Bay. In opposite to 'Eo' simulations, the 'Ei' experiments are running with modern orography but Pliocene ice sheets. That includes removed ice from Southern Greenland and East Antarctica and ice limited to high elevations in the East Greenland mountains. Pliocene ice sheets, land-sea-mask, topography and bathymetry are provided with the Pliocene Research, Interpretation and Synoptic Mapping (PRISM) data set. 'Eoi' simulations include the Pliocene orography and ice sheet.
Another characteristic of the experiments are superscript numbers ranging from 280 to 560 which indicate the prescribed concentration of CO_2 in units of ppmv. Together with the other atmospheric trace gases N_2O and CH_4 the CO_2 concentration is part of the boundary conditions. While the CO_2 can vary between 280, 350, 400, 450 and 560 ppmv for each simulation, the concentration of N_2O and CH_4 is kept constant during every experiment. Those CO_2 concentrations were selected, because 280 ppmv represents the PI state, 560 ppmv is the doubled value for estimation of climate sensitivity, 400 ppmv as the core experiment based on an updated best guess of CO_2 for the relevant period, and 350 as well as 450 ppmv to reflect uncertainty for the best fitting value of 400 ppmv. Table 3.1 gives a brief overview over all the experiments, with emphasis on the main simulations E^{280}, as reference, and Eoi^{400} as experiment, that are mostly used in this Bachelor thesis.

experiment	orography	icesheet	CO_2 concentration
E^{280}	present day	present day	280 ppmv
E^{400}	present day	present day	400 ppmv
Eoi^{280}	Pliocene	Pliocene	280 ppmv
Eoi^{400}	Pliocene	Pliocene	400 ppmv

Table 3.1: The four used experiments in this thesis set up and run by the Department for Climate Science, Paleoclimate Dynamics, AWI with COSMOS. Pliocene and present day icesheet and orography are further described in the text.

According to Dowsett et al. (2016) the newest data set by the PRISM, the so called PRISM4, stores paleogeographic and cryospheric components such as topography and bathymetry. Those conditions are based on a global relief model, ETOPO1, presenting the Earth's surface with integrated land topography and ocean bathymetry. Another content of this data set is the ice sheet distribution. With an overall reduction of ice sheets in terms of volume and extent, the Pliocene Greenland Ice Sheet was only about 25% of PI amounts. Most of Greenland was at a lower elevation due to a restriction of ice to high elevations of the Eastern Greenland mountains. Antarctica was not changed intensely with a lower elevation near the coast and most parts of West Antarctica, but a positive elevation near the South Pole.

3.2 Components of the COSMOS model

According to Stepanek and Lohmann (2012), the COSMOS consists of three models, each representing a component for the global domain. The model ECHAM5 is the atmosphere model, JSBACH represents land surface and vegetation, and MPI-OM models the ocean. Ocean and atmosphere are coupled by OASIS3, which is also part of the COSMOS. The following chapters 3.2.1 and 3.2.2 will describe the models ECHAM5 and JSBACH more detailed, while there won't be taken a further look on the MPI-OM module as well as the coupler OASIS3, since the results of this model are not part of the atmosphere-vegetation analysis in this work.

3.2.1 Atmosphere model ECHAM5

The ECHAM5 model operates in the configuration employed here, an T31/L19 grid with 19 levels up to 10 hPa. The grid has a horizontal resolution of 3.75°x3.75°. The ECHAM5 uses a spectral dynamic core and energy input by the top of atmosphere insolation, which is determined by orbital parameters and solar constant. These are all kept constant for the modelled time, independent whether it is a Pre-Industrial or Pliocene model run. This makes sense since the selected shortterm time slice has a strong similarity in orbital parameters to modern conditions. The atmospheric trace gases N_2O

and CH_4 can be adjusted as boundary condition, but will be kept constant for all the experimental runs. While the CO_2 concentration is varying depending on the experiment being used, the gases N_2O and CH_4 are set to 270 ppbv (parts per billion by volume) and 760 ppbv.
The atmospheric general circulation model mostly developed by the Max Planck Institute for Meteorology (MPI-M), can be run either standalone or coupled to the ocean by the OASIS3 coupler. For the PlioMIP2 set up it is always coupled. Atmosphere and land surface are not coupled but rather are linked by an implicit scheme. This scheme takes snow computed by ECHAM5 into account, as well as soil albedo and vegetation cover by JSBACH which play a crucial role in the Earth's energy budget.
The Pliocene T31/L19 set-up of the ECHAM5 model was implemented with boundary conditions, one among them is an adjusted land-sea-mask. For the Pliocene experiments, with the paleogeographical features mentioned in section 3.1, the land-sea-mask is changed as shown in Figure 3.1

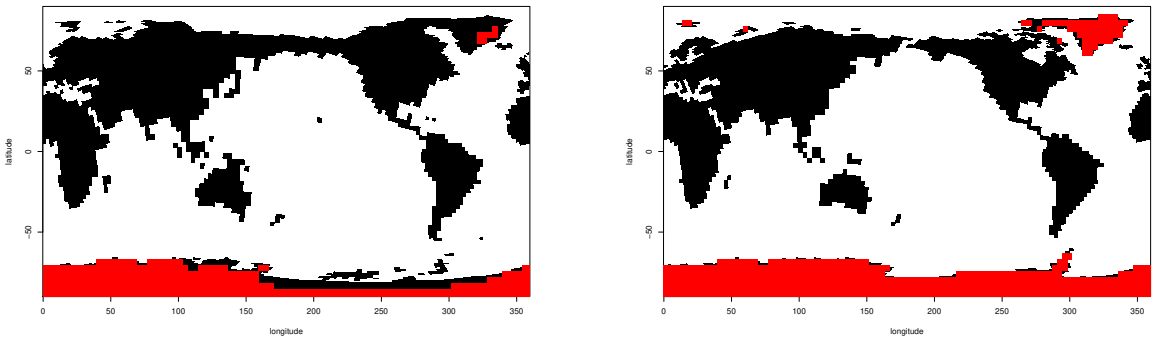

(a) (b)

Figure 3.1: The differences of the land sea masks and glacier mask (red) of the (a) Eoi- or (b) E-experiments. Biggest Pliocene changes are the closed Bering Strait, the closed Hudson Bay and some adaptations in Western Antarctica as well as Australia and Papua New Guinea.

3.2.2 Land surface and vegetation model JSBACH

The so called JSBACH is an extension of the ECHAM5 model and runs on the same 3.75°x3.75° grid (Raddatz et al., 2007). Many boundary conditions are adopted from the atmosphere like the land-sea-mask (refer to figure 3.1). According to Stepanek and Lohmann (2012) the land component JSBACH has implemented 13 plant functional types (PFTs), but only eight of them are used for the PlioMIP-modelling with COSMOS. For Phase 2 of the project, the same eight PFTs are used. They range from tropical evergreen trees to deciduous shrubs, also including two grass types. As PFTs will play an important role for this study, table 3.2 provides an overview of the eight PFT simulated by the model for PlioMIP2. Due to relatively common characteristics

level	PFT	type	climatic characteristics
1	tropical evergreen trees (TET)	forest	hot and wet conditions
2	tropical deciduous trees (TDT)	forest	warm and wet as well as dry conditons
3	extratropical evergreen trees (EET)	forest	cold and dry in winter, warm and moist in summer
4	extratropical deciduous trees (EDT)	forest	warm summer, cold winter and evenly spread precipitation over year
5	raingreen shrubs (RS)	grass	dry with short rain periods and warm to hot conditions
6	deciduous shrubs (DS)	grass	dry and temperate to cold conditions
7	C3 perennial grass (GC3)	grass	cool and moist conditions
8	C4 perennial grass (GC4)	grass	warm and dry conditions

Table 3.2: The eight different PFT used in the JSBACH model in COSMOS (Reick et al., 2013). The PFT were subjectively classified as "forest" or "grass" types depending on similarities in characteristics like albedo. By specific climatic conditions following Walter (1973) and Prentice et al. (1992) these types can be compared to existing biomes.

between some of the PFTs they were most times divided into forest- and grass-types in this thesis (Table 3.2).
Furthermore, JSBACH is implemented as a dynamic vegetation module, so that vegetation reacts to climatic conditions given by the ECHAM5 model. Since plants react to the conditions they must not be predescribed throughout the whole simulation. There is an initial distribution of, soil wetness, snow cover and a surface temperature climatology, which then develops during the simulation according to climatic changes by the ECHAM5.

4 Statistical parameters

4.1 Significance test

Testing the significance of the results is done by significance tests. Chosen for this thesis was the χ^2 Test as it does not rely on a normal distribution. This test analyses a coincidental or more than coincidental difference of two distributions by comparing them in classes with $n > 0$. For modelling, such tests are important because they show whether the results are significantly different from each other. The Pearson's Chi-squared test is defined by Schoenwiese (1985) as

$$\chi^2 = \sum \frac{(H_k(x) - H_k(y))^2}{H_k(y)} \tag{4.1}$$

with H_k being the frequency of occurence in the classes k, x the distribution of the observed value, in this case of simulation E^{280}, and y the distribution of the expected value, here of mid-Pliocene main core experiment Eoi^{400}.

4.2 Correlation

To determine whether the occurences of two modeled results are coincidentally or whether there is a correlation and dependence between the variables, a correlation coefficient can be computed. As the data points in the researched regions are quite few a first insight is derived with the coefficient of determination R^2. It is the part of the whole variance which is explained by the variable a (Storch and Zwiers (1999)).
With i being the number of grid points, $\bar{a}$ being the mean of the observed variable a and $\hat{a}$ being the prediction of the observed variable, the equation is:

$$R^2 = \frac{\sum (\hat{a}_i - \bar{a})^2}{\sum (a_i - \bar{a})^2} \tag{4.2}$$

As it depends on the number of explaining variables in the model, the adjusted R^2 is used in this work. It only rises with a high impact of the variable a, not by adding independent

variables which would be the case for the unadjusted coefficient of determination (Storch and Zwiers (1999)). The significance is hereby given by the p-Value.

5 Results

5.1 Equilibration of Eoi400 and E280

Models are usually run for a long time to reach an equilibrium state. With big adaptation from modern to Pliocene geograph, the different systems in the model need time to reach a state of balance, just like in the real earth system. Only when the simulation has run long enough to reach such a state, the situation is described best and shows most likely only the changes in the variables rather than big variances due to ongoing equilibration. Timeseries plots give an insight into the state of balance, showing whether the variables are still evolving or can be analysed with less variance in results. Even though the COSMOS includes three models (refer to Chapter 3.2) only the quasi-equilibrium states of JSBACH (vegetation model) and ECHAM5 (atmosphere model) are further described, with no consideration of the MPI-OM (ocean model) state.

5.1.1 Plant functional types indicating the state of the biosphere

Figure 5.1 shows the development of the vegetation types to give an overview of the JSBACH model's equilibrium state. While the modern day configuration of simulation E^{280} in Figure 5.1 (a) shows change of the grass and forest types throughout the simulated years, the Pliocene grass and forest in Figure 5.1 (b) experience greater changes. The use of the last 100 modeled years (2650-2749) in following analyses is because they represent a relatively stable state. With small remaining slope in both vegetation graphs for both simulations. Reduction of trends, defining an equilibrium state, occur much faster in the pre-Industrial time period after almost 1000 modeled years. Eventually, grass fraction decreases from the implemented vegetation distribution from about 0.43 to 0.41 while the forest types show almost no changes and keep their fraction of about 0.37. The Mid-Pliocene model shows a different trend in Figure 5.1 (b). Even though the implementation is similar to the pre-Industrial one, with the forest type starting at about 0.37, grass is at about 0.51, but fastly decreases to 0.43 for the last 100 years. Significant changes also occur in the forest vegetation, which continuously increases in the first 500 modeled years. Reaching a quasi-equilibirium state for Pliocene geography take up about 1300 years and results in almost the same fraction for grass and forest.

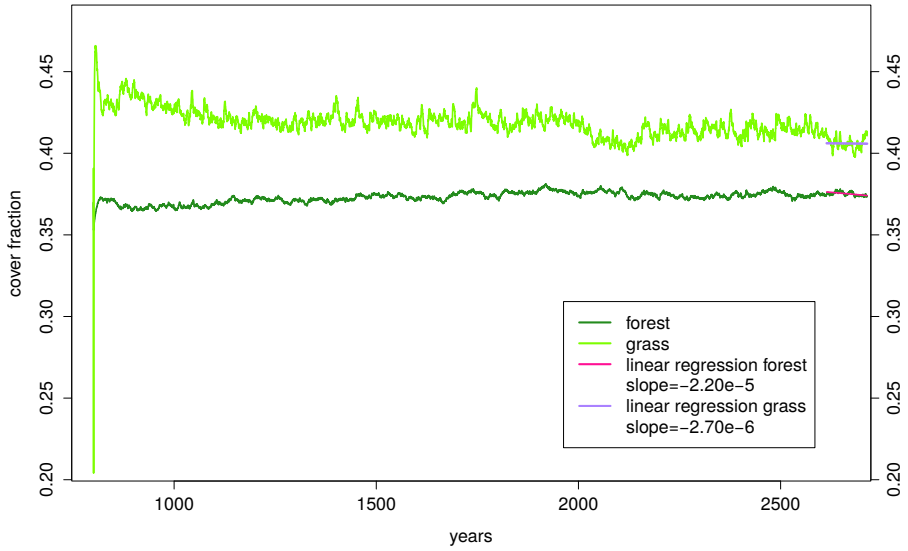

(a)

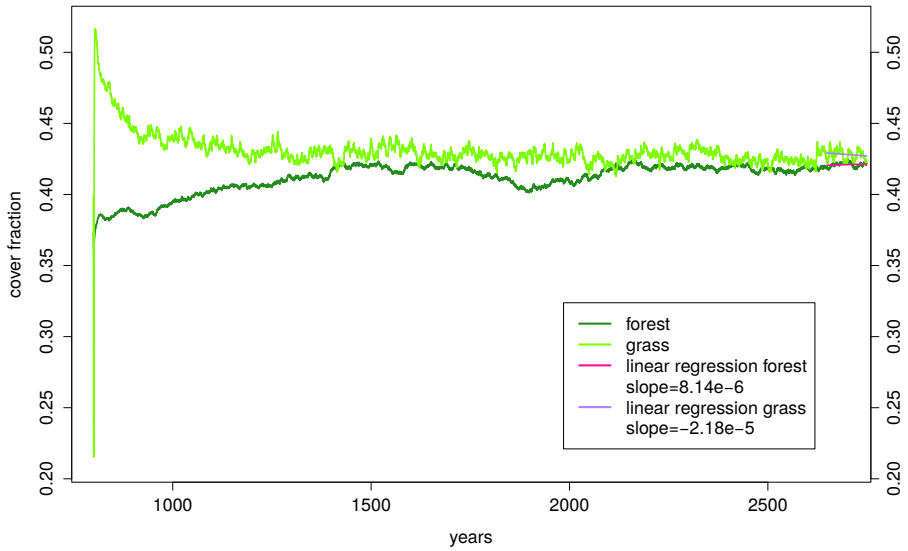

(b)

Figure 5.1: Timeseries (years 800-2749) of development of the vegetation cover expressed as grass- and tree-types (see Chapter 3.2.2 for more details) for both, (a) reference E^{280} and (b) Mid-Pliocene core experiment Eoi^{400}. The vegetation cover fraction is the sum of the proportion of the PFTs they hold in each grid cell which is then averaged over a global field including ice sheets.

5.1.2 Temperature indicating the atmosphere's state

Analysing timerseries of the temperature development gives an insight into the atmosphere models state of equilibrium.

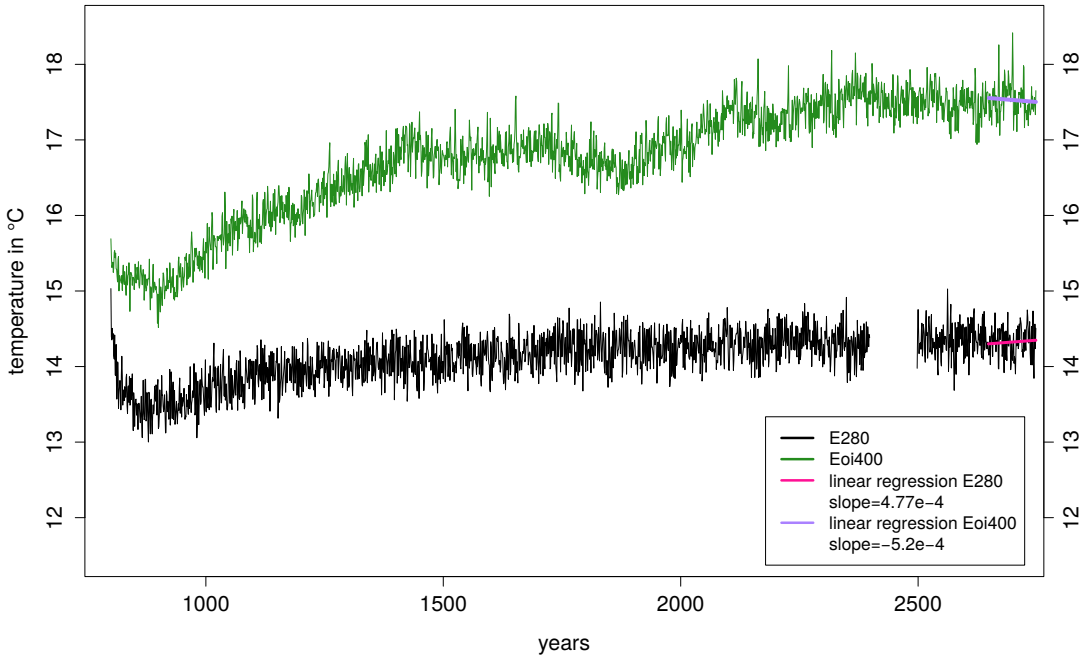

Figure 5.2: Timeseries of development of surface air temperature in both simulations E^{280} and Eoi^{400}. The gap in the E^{280} series is caused by errors in post processing, which led to missing data.

The temperatures in Figure 5.2 develop differently for simulations E^{280} and Eoi^{400} although they are initially close to each other at about 15°C. While the global surface air temperature in E^{280} drops for the first 100 years, it stabilizes at approximately 14.4°C after 1000 modeled years. The Mid-Pliocene simulation Eoi^{400} indicates an quasi equilibrium, similar to the vegetation model reached later than the other at the year 2500 which results in an increase in temperature over 2°C to more than 17°C.
Choosing the last 100 modeled years for the further analyses is mostly dependent on the Mid-Pliocene core experiment's equilibration, which takes more time for both, atmosphere and biosphere. Even for the pre-Industrial reference simulation the slopes are not 0 so there is still a variation, but with slopes of about 10^{-4} to 10^{-6} the climate states are already relatively robust. Not taken into account is the ocean's equilibrium state, which may not have been reached in those almost 2000 modeled years.

5.2 Atmosphere climatological data

5.2.1 Global surface temperature

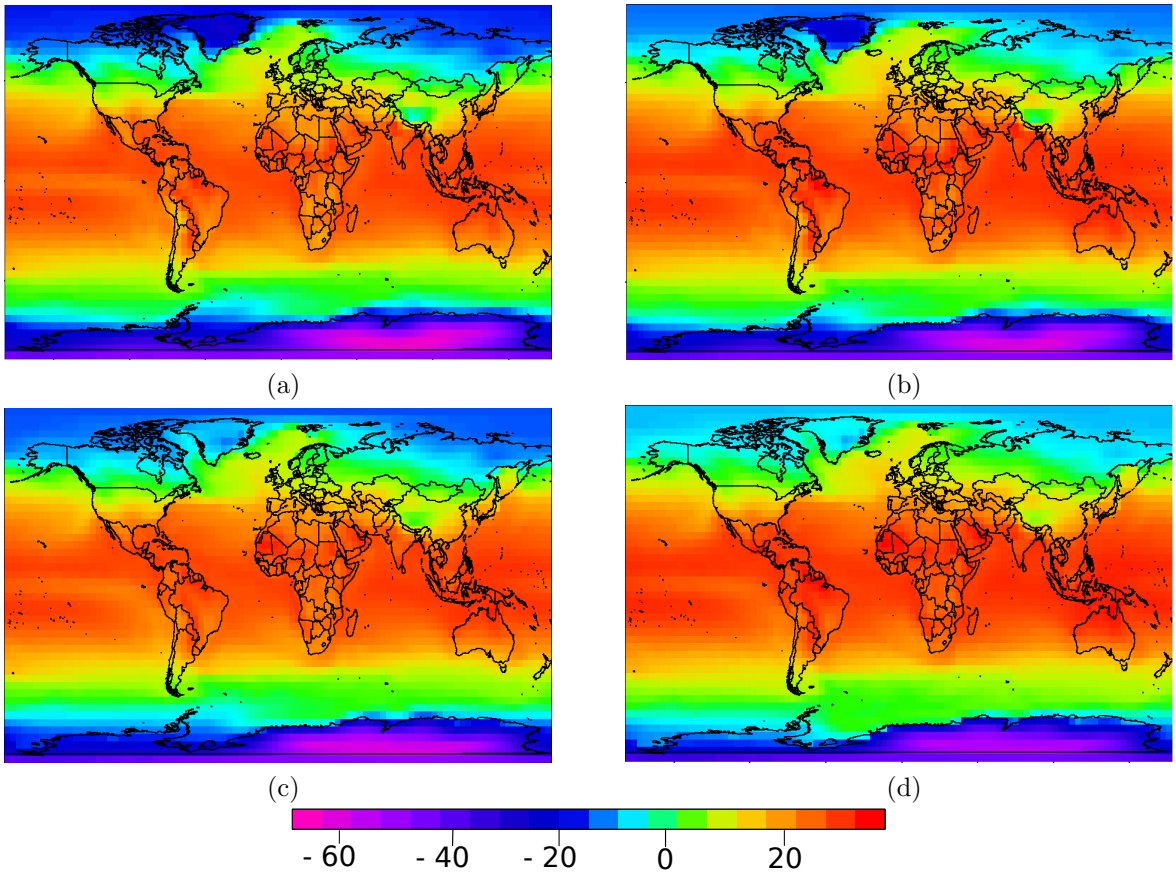

Figure 5.3: Global 100-year-averaged surface temperature in °C of simulations (a) E^{280}, (b) E^{400}, (c) Eoi^{280} and (d) Eoi^{400}. The land borders to not represent the Pliocene state, but rather are for easier comparison with the PI state.

As seen in Figure 5.3 and Figure 5.4 all four simulations E^{280}, E^{400}, Eoi^{280} and Eoi^{400} show an overall similar temperature distribution. With arrangements in the CO_2 concentration a shift into warmer climate is visible, while changes in paleogeography also cause a warming, but in the same global distribution. Especially on the ice sheets changes in paleogeography have a warming effect which may explain the different maximum and minimum temperatures in the simulations. While the lowest temperature for E^{280} is -77°C, E^{400} and Eoi^{280} only reach -73°C and Eoi^{400} 10°C more with -67°C. This shift to warmer climate is also visible in the maxima with 43°C (experiment E^{280}), 45°C (experiment E^{400}), 46°C (experiment Eoi^{280}) and 49°C (experiment Eoi^{400}). Most of the highest temperatures over 30°C occur in simulation E^{400} with about 2000 counts difference to Eoi^{400}. Both simulations are shifted to 2°C higher temperatures than both simulations

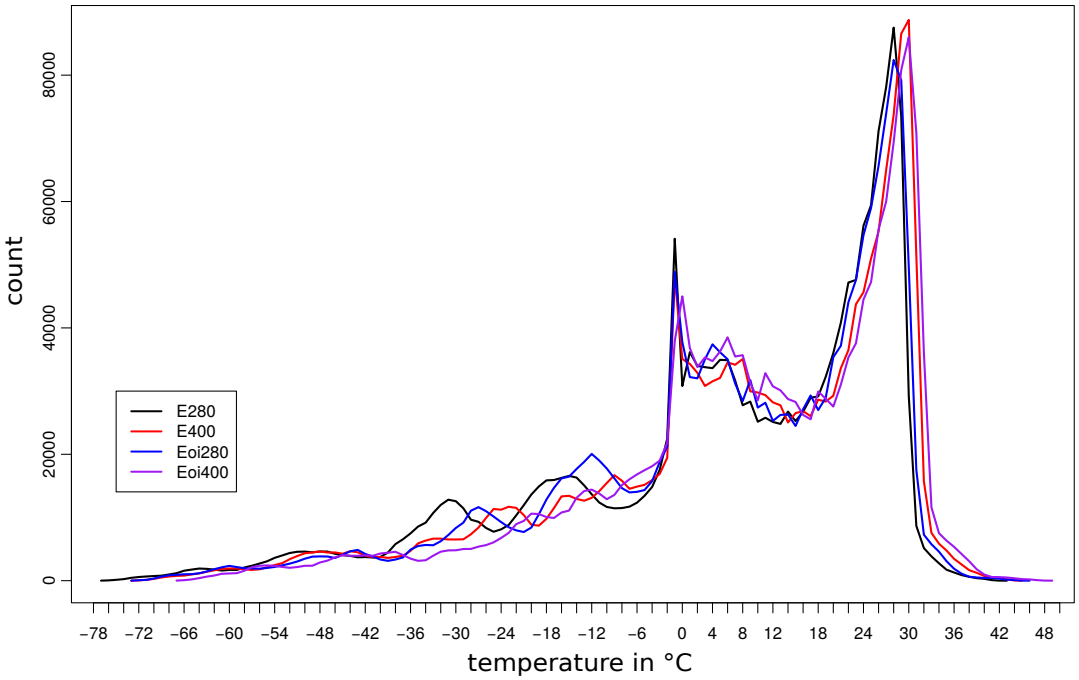

Figure 5.4: Count of grid cells (histogram) rounded to 1° in which the surface air temperature in the simulation E^{280}, E^{400}, Eoi^{280} or Eoi^{400} occurs. The global surface air temperatures are a seasonal mean of all four seasons of 100 model years (2650-2749).

using 280 ppmv CO_2. In a global average of the surface air temperatures the differences to 14.33°C in E^{280} are 0.88°C in Eoi^{280}, 2.05°C in E^{400} and 3.20°C in Eoi^{400}.

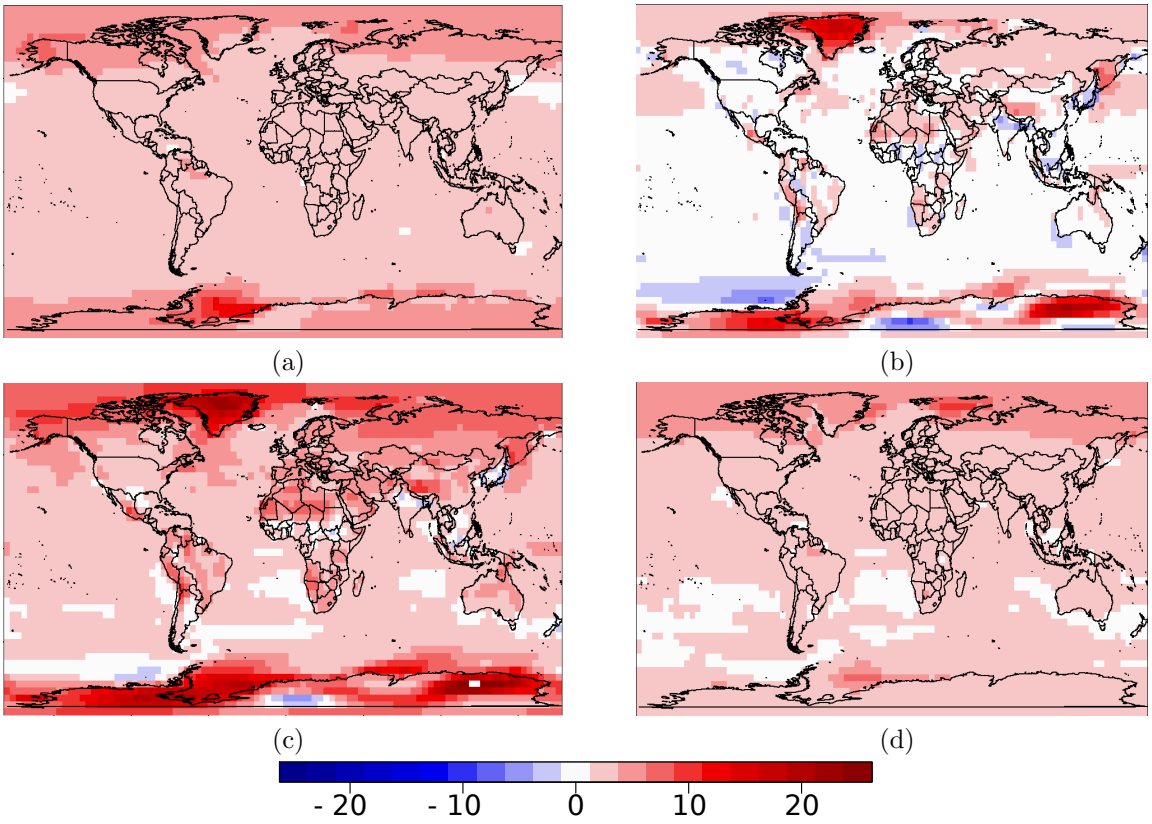

Figure 5.5: Global surface air temperature anomalies in °C. The 100 year mean difference is shown for (a) Eoi^{400} - Eoi^{280}, (b) Eoi^{280} - E^{280}, (c) Eoi^{400} - E^{280} and (d) E^{400} - E^{280}. The land borders to not represent the Pliocene state, but rather are for easier comparison with the PI state.

With Figure 5.5 showing global anomalies between different simulations, a more regional analysis is possible, even though all four differences show a positive temperature anomaly. Only Figure 5.5 (b) displays prominent partial cooling with more than 10°C in the Southern Hemisphere. Overall (a) gives information about influence of CO_2 concentration with a paleogeographical world of the Mid-Pliocene, (b) shows the changes of temperature due to changes in orography and ice sheets, (c) differences of changing the paleogeography and CO_2 and (d) only changes in CO_2 concentration in a modern geography. Figure 5.5 (a) and (c) show a warming on a global scale with a focus on high latitudes. With the Mid-Pliocene geography higher temperatures up to 14°C occur especially in Antarctica, while the biggest warming with modern geography concentrate in high latitudes on the Northern Hemisphere with up to 12°C in Barents Sea. With only adjustments in geography as in Figure 5.5 (b) big warming of almost +24°C appear especially in the adapted ice sheets on Greenland and West Antarctica. But in Antarctica and surrounding areas also negative anomalies occur in the South Pole and

Bellinghausen Sea of -18°C. That changes of ice sheets or geography not only lead to surface temperature anomalies in the changed area but also in surrounding areas was already shown by Lohmann et al. (2015) with rising temperatures with removal of inland ice in Greenland. In low latitudes are slight anomalies in positive as well as negative trends or no difference at all. The changes occuring in Figures 5.5 (a), (b) and (d) are merged in (c) showing the difference of the main core experiment Eoi^{400} and pre-Industrial representing E^{280}. Warmings of widespread 15 to over 25°C in high latitudes especially on Greenland and Antarctica are computed. The decreasing temperatures, that occured in (b), are also part of the global surface air temperatures in (c) where in the area of the South Pole and Bellinghausen Sea up to 5°C less. The low latitudes show moderate warmings of about 5°C with some exceptions where no changes occur.

5.2.2 Global net-precipitation

For the growth of plants not only temperature but also precipitation has an influence and vice versa. Further net-precipitation, that is the difference of precipitation and evaporation, helps to determine where precipitation reaches the ground. While by observation the vegetation of mid- to high latitudes is primarily due to changes in temperature, precipitation is the main driving factor for tropical and subtropical vegetation (Liu et al. (2006)).

Strongest differences between Mid-Pliocene, represented by Eoi^{400}, and PI, simulation E^{280} occur according to Figure 5.6 (a) in low latitudes near the equator. There anomalies of up to 2m are widespread with a focus on a band reaching from the coast of Eastern Africa to the Western Pacific. Differences in net-precipitation are small or non existent over the continents, apart from high latitudes on the Northern Hemisphere, where there is about an additional 1m precipitation reaching the ground in the simulation Eoi^{400}. Those differences are not occuring because of different global patterns that may have evolved, but rather varying strenghts in the simulations (see Figure 5.6 (b) and (c)). Global distributions are very similar although the highest anomalies are computed at the border of changes from more to less net-precipitation like in the Northern Indian Ocean, where on a small scale the net-precipitation changes from -2 to +3m/year. An absolute value of 2 or 3m/year is hereby a significant change as globally maximum values of ±3.5m/year were computed.

5.3 Vegetation data

With changes in the atmospheric variables, vegetation distribution should also change, which is the case as already seen in Figure 5.1. Hereby it is important to not only take a look on the global scale but also on regional as the vegetation types differ as well as temperature or precipitation and feedbacks or correlations are better understandable on

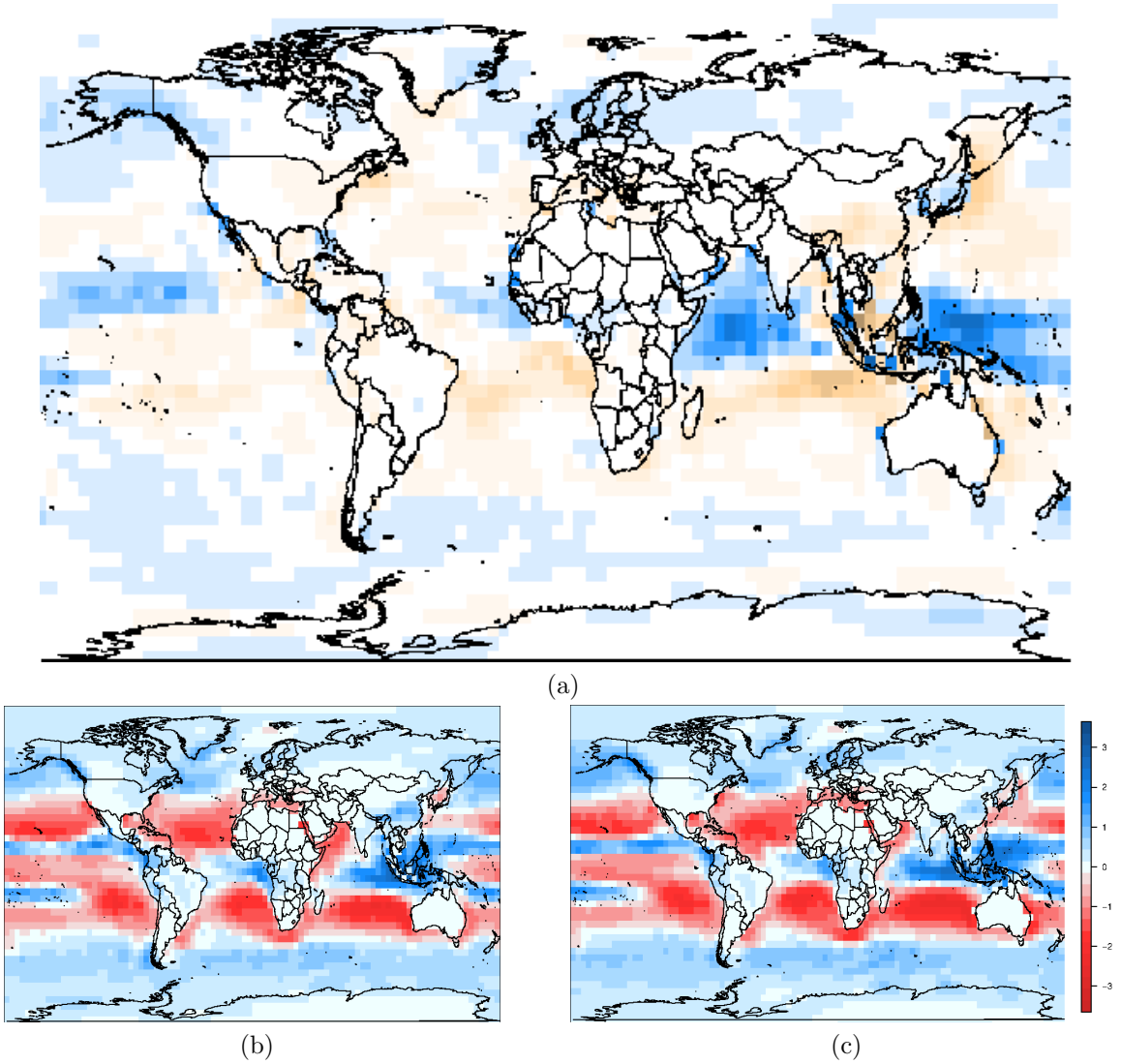

(a)

(b)

(c)

Figure 5.6: Shown are (a) anomaly of global net-precipitation, that is the difference of precipitation and evaporation, in m/year of E^{280} and Eoi^{400}, (b) the net-precipitation distribution of E^{280} as well as (c) the distribution of Eoi^{400}. The land borders to not represent the Pliocene state, but rather are for easier comparison with the PI state. Shown is the mean of the last 100 modeled years (2650-2749).

a smaller scale. This Section does not only analyse the global differences in vegetational patterns but also concentrates on a region where big changes occur.

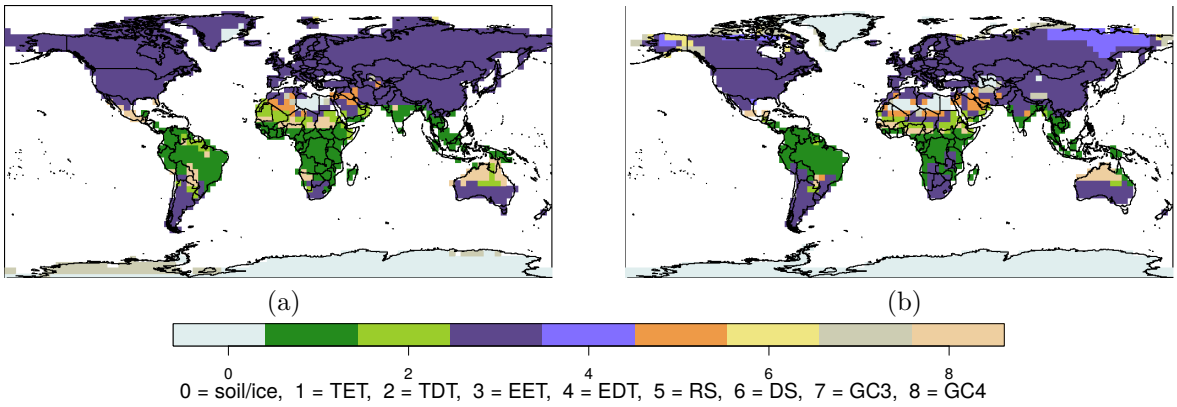

Figure 5.7: Dominant PFT of (a) Eoi^{400} and (b) E^{280}.

5.3.1 Global vegetation distribution

Simulations with changes in boundary conditions such as ice sheet and orography as well as CO_2 concentration show a difference in the global grass (Figure 5.8) and forest (Figure 5.9) distribution. The mid-Pliocene adaptations in orography and ice sheet, which are Figures 5.8 (b) and (d) for the grass fraction allow growth in Greenland and West Antarctica due to removing the ice sheet (see Section 3.1) but also more area to grow because of the closed Bering Strait and Hudson Bay. These regions are highly covered by grass with up to almost 100% on the Bering Strait and up to 90% on Greenland for the simulation Eoi^{280}. Figure 5.9 (d) showing simulation Eoi^{400} also displays more than 50% of grass fraction in the areas mentioned above, but the increase in CO_2 permits a global decrease of grass which is focused on high latitudes. It does not change the global spatial distribution patterns.
In the modern day configuration of simulation E^{280} in Figure 5.9 (a) more than 50% of vegetation is forest type along the equator and mid- to high latitudes which can be classified into the tropical and extratropical tree types. In Figure 5.9 (b) of simulation Eoi^{280} there are almost no changes to simulation E^{280} (Figure (a)) in low latitudes and Antarctica, but a small expansion north on the Northern Hemisphere is visible with focus on Greenland. With only rising CO_2 concentration in simulation E^{400}, Figure 5.9 (c), there is a similar picture to Eoi^{280} without the vegetation on Greenland with slight changes in Northern Russia and Canada to a more Northern spreading of forest. With the combination of both, adaptations in paleogeography and CO_2 as in (d) of simulation Eoi^{400} the northward spread of forest is most distinct. With slight negative changes along the equator.

A better visualisation of the differences between simulation Eoi^{400} and E^{280} is given by Figure 5.10 showing the anomaly of grass (in Subfigure (a)) and forest (in Subfigure (b))

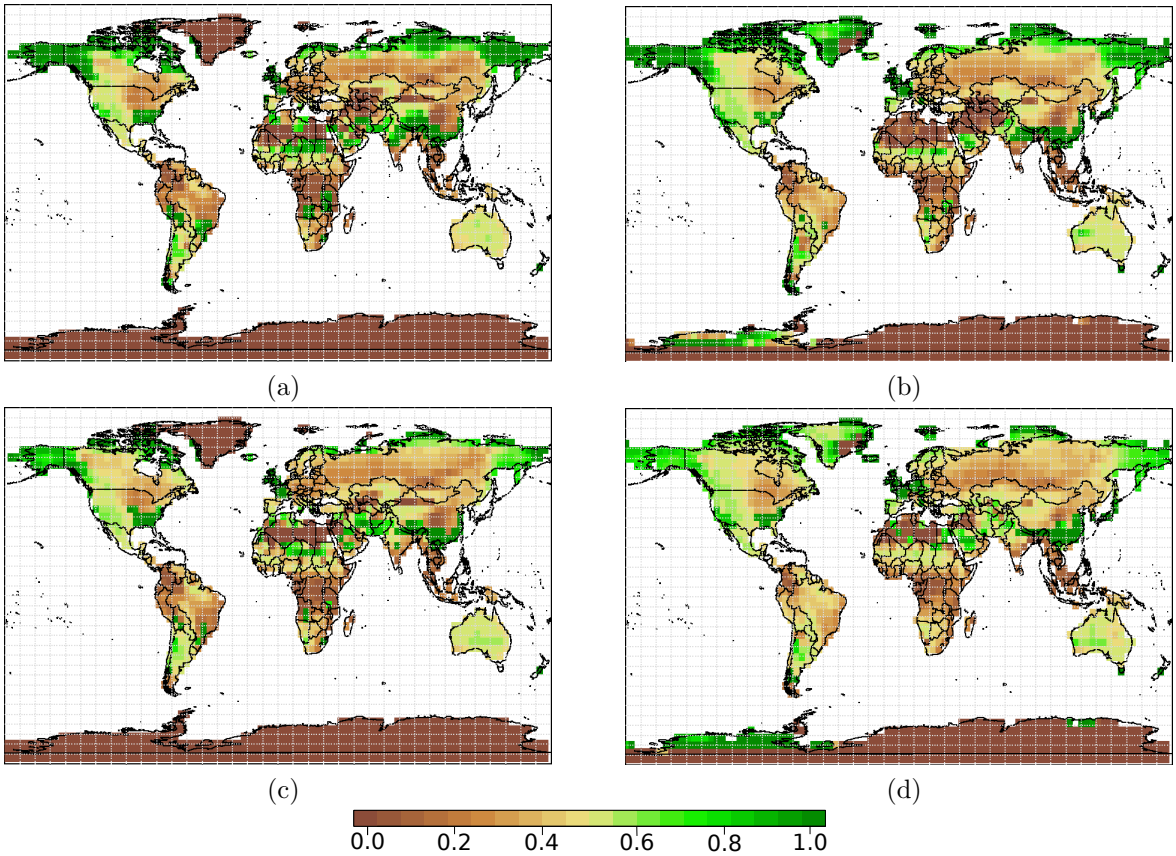

Figure 5.8: Global vegetation distribution as 100 year mean (2650-2749) of the grass fraction (see Chapter 3.2.2). Shown is (a) grass fraction of E^{280}, (b) grass fraction of Eoi^{280}, (c) grass fraction of E^{400} and (d) grass fraction of Eoi^{400}. The land borders to not represent the Pliocene state, but rather are for easier comparison with the PI state.

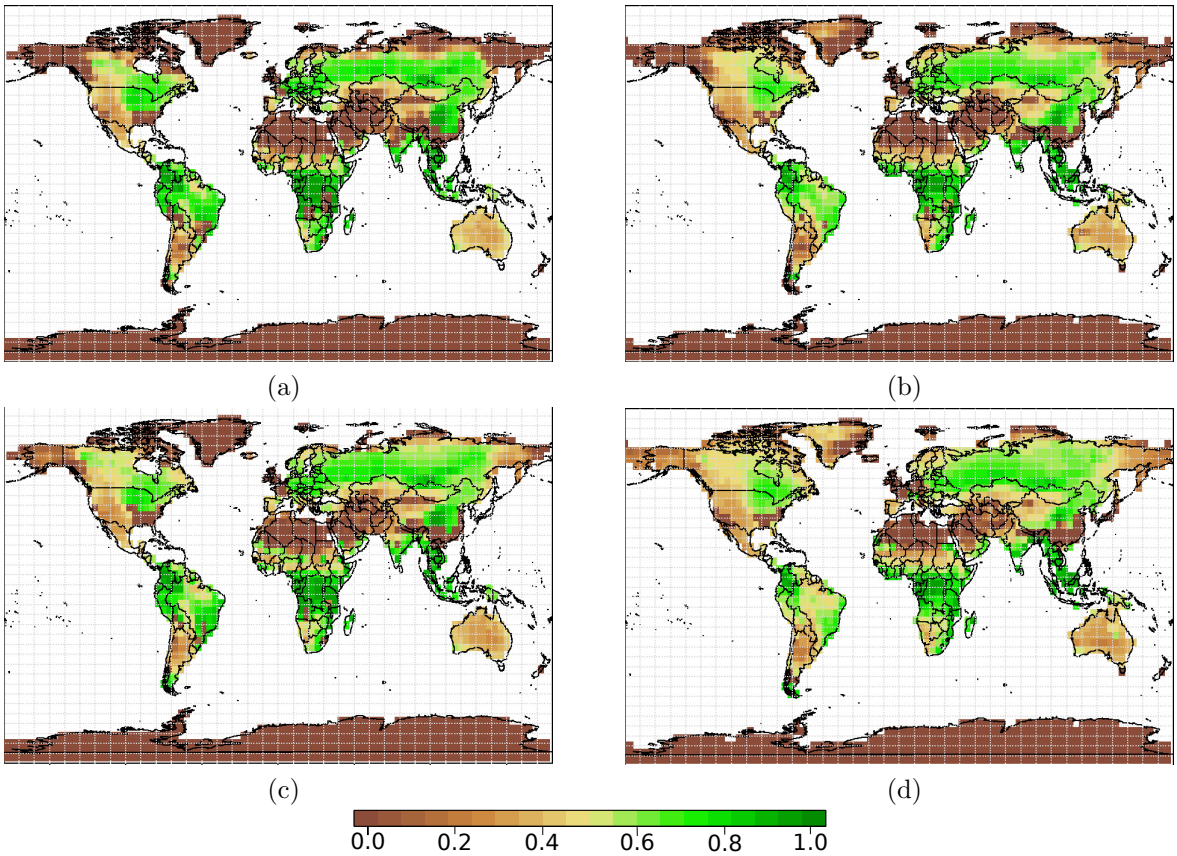

Figure 5.9: Global vegetation distribution as 100 year mean (2650-2749) of the forest fraction (see Chapter 3.2.2). Shown is (a) forest fraction of E^{280}, (b) forest fraction of Eoi^{280}, (c) forest fraction of E^{400} and (d) forest fraction of Eoi^{400}. The land borders to not represent the Pliocene state, but rather are for easier comparison with the PI state.

fraction. The biggest changes of grass and forest are mostly proportional. When the grass fraction increases like in North of South America and South Africa, the forest fraction decreases, whereas in areas with increasing forest fraction, like in Northeast Russia and Alaska, the grass reduces in the same amount forest gains. The only exceptions are former ice sheet regions, that include Greenland and West Antarctica with an increase of grass and forest vegetation in Greenland and an increase of grass without growing trees in West Antarctica.

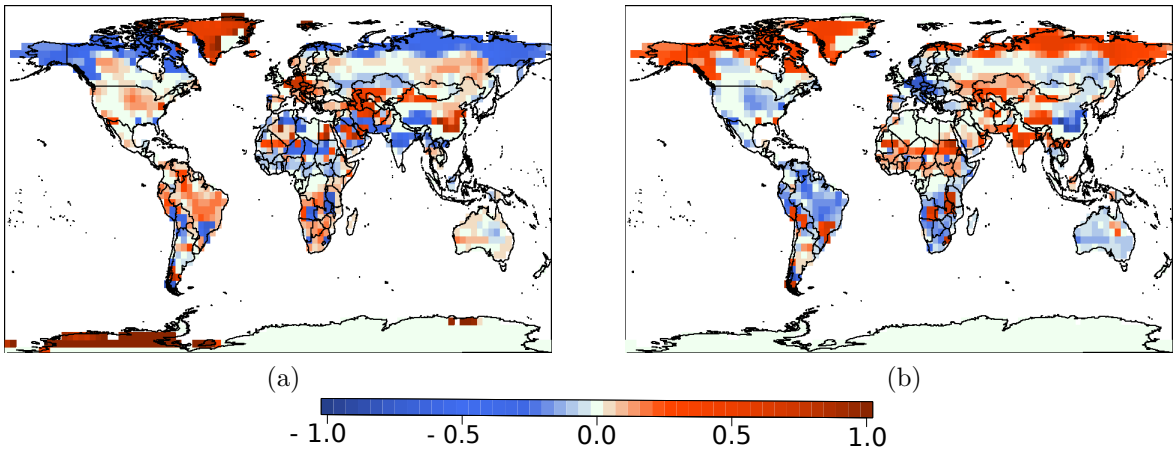

Figure 5.10: Vegetation anomaly of (a) grass and (b) forest fraction covers of reference E^{280} and Eoi^{400}. The land borders to not represent the Pliocene state, but rather are for easier comparison with the PI state.

The changes in vegetation types (Figure 5.10) give altogether a good overview of the Mid-Pliocene vegetation distribution. There is a change from ice sheet to boreal forest but also grass on Greenland, a change from desert to grass on the Arabian Peninsula, a decrease of forest type while increasing grass types in the rainforest, a retraction of subtropical - and semi-deserts in Sahel zone where there is in parts a spread of grass and a northward shift of forest and grass types, a clear northward shift of forest in expense of grass on the Northern hemisphere, a growth of almost 100% of grass on the removed ice sheet on West Antarctica and an increase of grass on the European continent

5.3.2 Shift in Northern Hemisphere treeline

The northward shift of the forest type is one of the most significant changes between pre-Industrial and Pliocene vegetation distribution. Due to its significance on the whole Northern hemisphere, a more detailed analysis of not only Eoi^{400} but also Eoi^{280} and E^{400} is needed, as they should show agreement.

The northward distribution of especially forest types of vegetation is one of the main changes on which the findings for the mid-Pliocene warm period agree on. Therefore

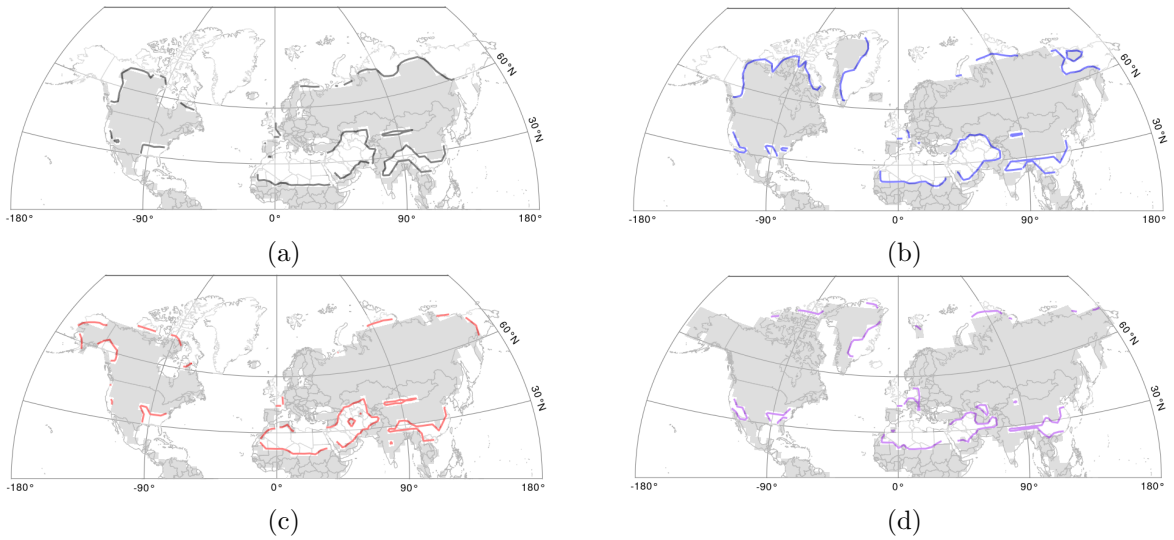

Figure 5.11: Treeline which is here defined as 10% of the forest PFT for (a) simulation E^{280}, (b) Eoi^{280}, (c) E^{400} and (d) Eoi^{400} with the shading indicating a forest vegetation fraction of more than 10%. The land borders to not represent the Pliocene state, but rather are for easier comparison with the PI state.

a further analysis of this extreme change in the simulation Eoi^{400} as well as Eoi^{280} and E^{400} may show agreement.

The different distributions of forest type vegetation including tropical and extratropical trees are shown in Figure 5.11. In the modern simulation E^{280} the treeline of >10% forest fraction is restricted by the northern border of the American continent. In West Canada it almost follows the Northern Rocky Mountains. While it also follows the continent in Europe ending in Northern Scandinavia, forest does not reach the sea in Siberia and is not found in the Northeast of Russia. Simulation Eoi^{280} shows a clear northward shist of the treeline into the (now closed) Canadian Archipelago and Hudson Bay, covering the West of Greenland in Subfigure (b). The movement is also visible in Russia, now reaching the Arctic Ocean in the North, and Kamtschatka in the East. But not only the changes in high latitudes are displayed as there are also changes in Africa where forest vegetation starts to cover the coastal areas of the Sahel. Subfigure (c), showing the >10% forest fraction of E^{400}, marks a westward distribution from Canada over Alaska, reaching the Canadian Archipelago in the North. The northward shift is also visible in Europe and Asia, where the coast often has a more than 10% forest vegetation. In mid latitudes the change in CO_2 concentration leads to a southward spreading of forest at the Mediterranean region from Spain to Marocco. Over 10% forest vegetation almost cover the whole Northern Hemisphere in simulation Eoi^{400} which implies a shift in treeline into almost every direction. North America is totally covered except for small parts along the East and West coast of the US, almost reaching the Arctic Sea in the North, also covering most of Greenland with Eastern Greenland as exceptions since it is still iced. Even though there is less forest vegetation in Western Europe, it expands northwards

to Spitsbergen and eastwards over all Russia and Northern Asia over the closed Bering Strait to Alaska. In mid to low latitudes an increasing cover on the Arabian peninsula and therewith Northeastern coast of Africa is visible.

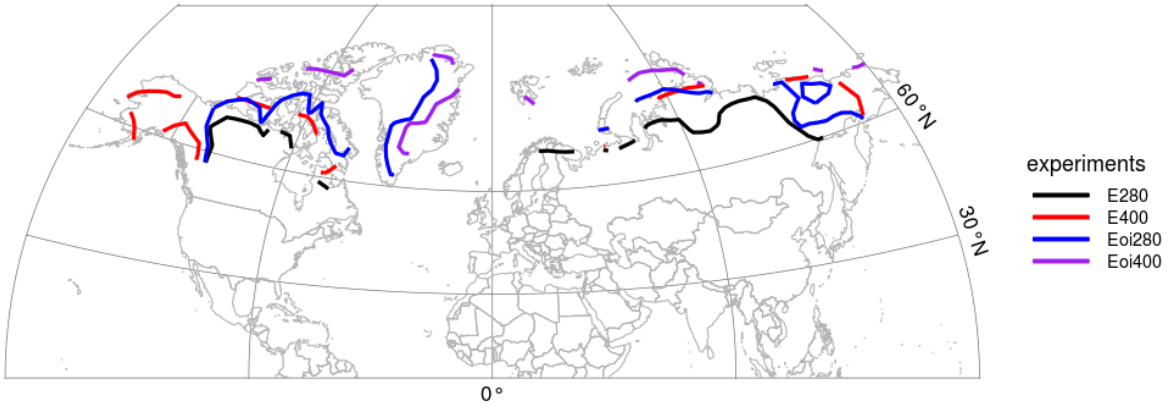

Figure 5.12: Northern Hemisphere treeline here defined as 10% of the forest group PFT in higher latitudes of the simulations E^{280}, E^{400}, Eoi^{280} and Eoi^{400}. The land borders to not represent the Pliocene state, but rather are for easier comparison with the PI state.

Concentrating on the treeline of the very North in Figure 5.12 a northward shift of all simulations compared to E^{280} is displayed. Clearly, the distribution is dependent on the ice sheet and orography configuration but even an enhanced CO_2 concentration shows a northward shift to the very possible. More noticeable is hereby the expansion to the West in North America, which reaches up to 1700 km, and to the East in Russia, which is about a 1000 km shift of the treeline. Therefore it may be concluded that in a direct and/or indirect way forest vegetation benefits of the CO_2 concentration. When adjusting the orography and ice sheet to the mid-Pliocene not only those regions experience a change but rather all continents. Nevertheless, simulation Eoi^{400} shows the furthest northward shift of forest. That includes a shift to almost 83°N on Greenland which indicates a shift of about 2200 km, a shift to 78°N on Europe, showing a northward expansion of about 1000 km and to almost 79°N in Siberia, leading to a shift of about 800 km.

5.3.3 Regional changes in vegetation

Although there are changes all over the globe, a regional analysis can explain local differences, making a first impression easier. For this thesis two regions as shown in Figure 5.13 were chosen and described in the following chapters. They are of importance as there are changes giving the opportunity to explain a variety of differences. The Siberian region has some of the highest temperature anomalies (see Figure 5.5c)) as it is located in the high latitudes. Also changes in the presence of dominant PFT occur (Figure 5.7), mostly diverging from EDT to EET as well as an overall increase of forest

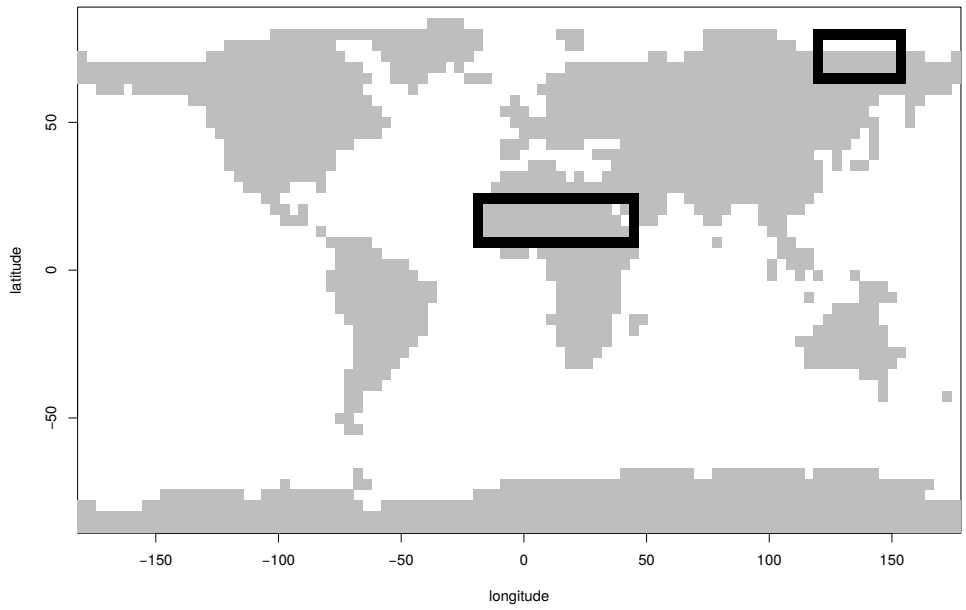

Figure 5.13: Shown is the land sea mask configuration for the JSBACH module. The black box in the center borders the region of Sahel Zone in Africa and the black box in the North-East indicates the part of Siberia which are analysed in this chapter.

type vegetation as seen in Figure 5.10. The African, more exact Sahel, region is not as consistant in its change and therefore local factors play an important role. Following Figure 5.10 there are more or less high increases or decreases of grass types, but also increases of forest fraction and also a northward shift of forest vegetation (Figure 5.11a) and d)). These local variances are also visible in the dominant PFT with an overall increase of vegetation coming together wth e.g. changes from RS to TDT. Both regions are not significantly influenced by changes in net-precipitation (see Figure 5.6).

Figure 5.14 gives an insight of the changes of each PFT in the Siberian region. While the types TET, TDT, RS and GC4 do not show any changes, which is due to those types not exisiting in the area, EET increases its area with EDT, DS and GC3 decreasing. The difference of Eoi^{400} to the reference E^{280} is not the highest value in every case, but it is clear that only changing the orography and ice sheet lead to a smaller change in vegetation. With the exception of a small increase of DS in the case of Eoi^{280} the trends are the same for each experiment. The adaptation of orography and ice sheet led to a bigger land area that is vegetated in the simulations Eoi^{280} and Eoi^{400}. Therefore looking at Eoi^{400}, the increase of almost 1.5 mio km^2 of EET exceeds the decrease of $\sim$0.4 mio km^2 of EDT in addition to $\sim$0.4 mio km^2 of DS and $\sim$0.5 mio km^2 of GC3. The values between the difference of E^{400} and Eoi^{400} to E^{280} are affected by small discrepancies with GC3 losing most of the area in the case of E^{400}, even more than in Eoi^{400}.

The areal differences in vegetation in the African Sahel Zone, as shown in Figure 5.15, are more interlaced than in Siberia as 6 of the 8 PFT are integrated. While experiments

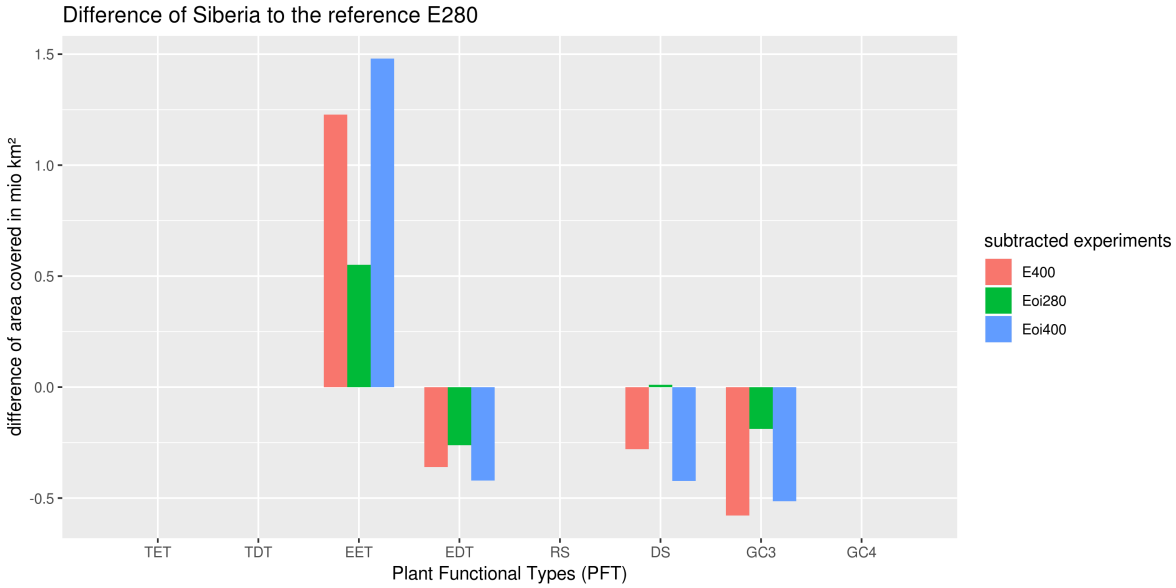

Figure 5.14: Anomaly of the Siberian region (see Figure 5.13) covered by each PFT from the experiments E^{400}, Eoi^{280} and Eoi^{400} to the reference E^{280}.

Figure 5.15: Anomaly of the Sahel Zone (see Figure 5.13) covered by each PFT from the experiments E^{400}, Eoi^{280} and Eoi^{400} to the reference E^{280}.

Eoi^{280} and Eoi^{400} show a significant decrease around -0.5 mio km^2 of RS and a small one of under -0.1 mio km^2 of EET, they have increasing areas of TET (about 0.8 respectively 1.45), GC3 (under 0.1 mio km^2) and GC4 (about 0.5 mio km^2 each). In the case of TDT they differ as Eoi^{280} shows a small decrease and Eoi^{400} a presentable increase which agrees with E^{400}. Overall E^{400} evidences smaller changes in vegetation cover by area as it includes an increase of 0.8 mio km^2 of TET, TDT and RS combined as well as a decrease of 0.2 of GC4. That shows an expansion of vegetation which is related to the higher CO_2 concentration but also a reversed trend.

5.4 Regional response of atmosphere and vegetation

5.4.1 Vegetation and temperature

For a first step in explaining the developments shown in the previous chapters, a correlation of the changes in vegetation and temperature of experiments Eoi^{400} and E^{280} is done. The anomalies of temperature in the areas of a) Siberia and b) African Sahel zone are plotted versus the anomalies of the occurring or most significant PFT. With the linear regression showing a trend, the coefficient of determination, tested with the p-Value (see Chapter 4), explains the correlation.

Siberia

In Figure 5.16 the four types of changing PFT, as shown in Figure 5.14, are correlated with the temperature anomaly between experiment Eoi^{400} and E^{280}. In the Siberian region EET shows a big increase which is significant but not highly correlated to the increase in temperature, with R^2 being 0.29. Even though the amunt decreases with rising temperatures all grid points are gaining EET. This goes along with the decrease of other PFT like EDT. This PFT is most correlated to temperature, R^2=0.72, including also some points with no changes, and highest decreases with lowest temperature increases. Therefore it can be concluded that the Decidious Tree acclimatises to high temperatures as no decrease occurs for temperature anomalies over 7.2°C. The only Siberian PFT whose change is not significantly correlated to the increasing temperature is DS with R^2=-0.033. While DS mostly decreases, a small number of grid cells show an increase in DS for high temperatures. A clear trend and significant high correlation (R^2=0.70) is between GC3 and the temperature as it steadily decreases with rising temperatures. With a small increase until an anomaly of 6.5°C it seems like the cold loving C3 grass reached its turning point at that temperature.

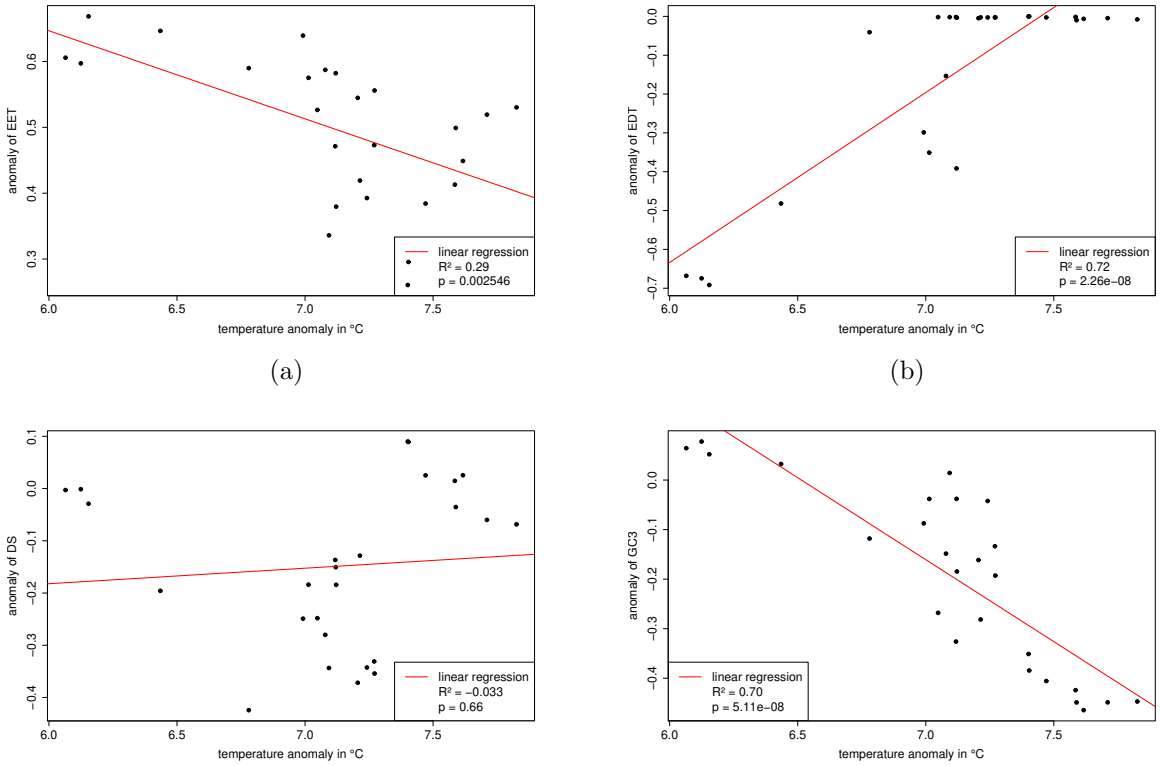

Figure 5.16: Changes in a yearmean of all four PFT that occur in the Siberian region from simulation Eoi^{400} to E^{280} versus the anomaly of surface air temperature. Figure (a) shows the anomaly of Extratropical Evergreen Trees (EET), (b) the anomaly of Extratropical Deciduous Trees (EDT), (c) the anomaly of Deciduous Shrubs (DS) and (d) the anomaly of C3 perennial grass (GC3). The red line indicates the linear regression, while the adjusted R^2 explains the correlation tested by the p-value.

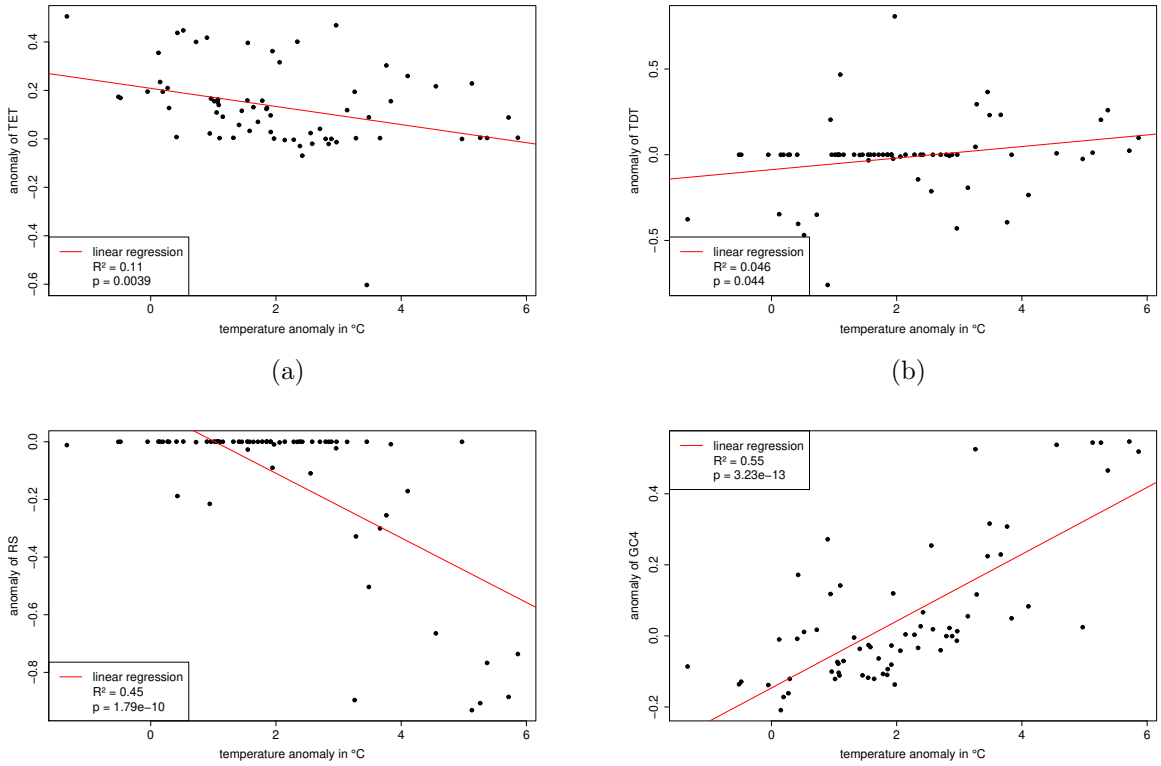

Figure 5.17: Changes in a yearmean of all four PFT that occur in the Sahel Zone from simulation Eoi^{400} to E^{280} versus the anomaly of surface air temperature. Figure (a) shows the anomaly of Tropical Evergreen Trees (TET), (b) the anomaly of Tropical Deciduous Trees (TDT), (c) the anomaly of Raingreen Shrubs (RS) and (d) the anomaly of C4 perennial grass (GC4). The red line indicates the linear regression while the adjusted R^2 explains the correlation tested by the p-Value.

Africa

In difference to the correlation of PFT and temperature in Siberia, the tree types occurring and changing in the Sahel Zone are not significantly correlated to the temperature, but grasses and shrub one. Following Figure 5.17 the types TET and TDT show very little similarities as TET is growing except for one grid cell and TDT is partly growing and declining independent of the temperature anomaly which shows mostly positive values with 4 exceptions where there is a negative temperature anomaly. Again RS having a significant correlation of 0.45 to the increasing temperature with highest decreases at highest temperatures shows that there can be a dependence even if many points are showing no change in vegetation, like in the case of TDT. The importance of temperature in the growing process is best visible for GC4. Its area steadily increases with rising temperatures, having its peak at the maximum of 6°C over reference. With a coefficient of determination of 0.55 it also demonstrates the biggest response of vegetation to temperature change in the Sahel Zone.

5.4.2 Vegetation and precipitation

The temperature is not the only variable having influence on the growth of vegetation. Precipitation is another example. Therefore, the correlation by the coefficient of determination and its p-value are computed for each of the PFT presented in Chapter 5.4.1.

Siberia

Other than the high and significant correlations between temperature and vegetation in Siberia, the vegetation and precipitation (presented in Figure 5.18) show, contrary to expectations, no significant relationship. Each correlation is smaller than 0.05. Similar to temperature the precipitation increases in the whole region, but not as strong. The weakness of the precipitation may cause the dissatisfying results of small correlations. Overall, as defined in the model, the vegetation does not respond to changes in precipitation of this size, which leaves the temperature as the main driving factor of both analysed variables in the Siberian region.

Africa

In difference to the Siberian region there are responses between vegetation and precipitation in the Northern African region. Those may may be caused by the higher values of precipitation anomaly (up to a factor of 10). Not all PFT show significant results as only the tree types, a) and b) of Figure 5.19, show an increasing trend for increasing precipitation for TET and a decreasing trend for TDT resulting in correlations of 0.39

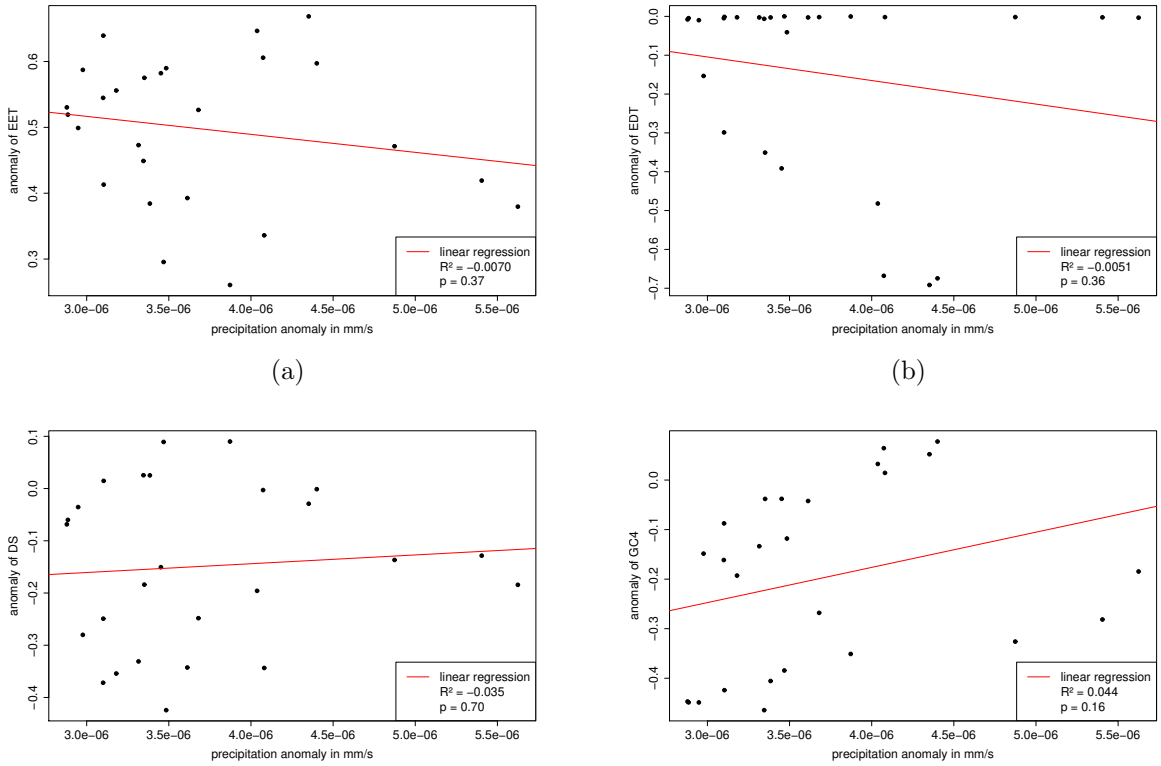

Figure 5.18: Changes in a yearmean of all four PFT that occur in the Siberian region from simulation Eoi^{400} to E^{280} versus the anomaly of precipitation. Figure (a) shows the anomaly of Extratropical Evergreen Trees (EET), (b) the anomaly of Extratropical Deciduous Trees (EDT), (c) the anomaly of Deciduous Shrubs (DS) and (d) the anomaly of C3 perennial grass. The red line indicates the linear regression while the adjusted R^2 explains the correlation tested by the p-Value.

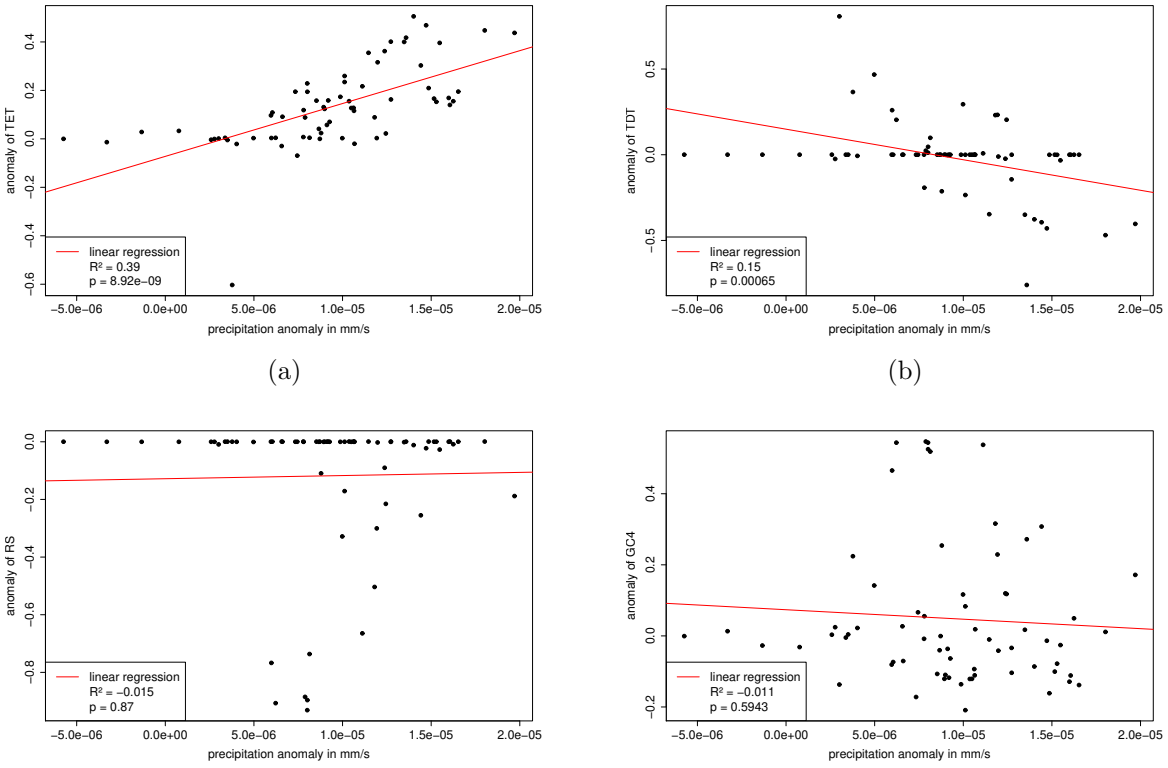

Figure 5.19: Changes in a yearmean of all four PFT that occur in the Sahel Zone from simulation Eoi^{400} to E^{280} versus the anomaly of precipitation. Figure (a) shows the anomaly of Tropical Evergreen Trees (TET), (b) the anomaly of Tropical Deciduous Trees (TDT), (c) the anomaly of Raingreen Shrubs (RS) and (d) the anomaly of C4 perennial grass (GC4). The red line indicates the linear regression while the adjusted R^2 explains the correlation tested by the p-Value.

respectively 0.15. Tropical tree types seem to be more responsive to precipitation, more than to temperature in difference to the grass types. Figure 5.19 c) and d) have no clear structure, especially GC4 which increases and decreases at the same value of precipitation anomaly. The result of RS not being correlated to the precipitation is most unexpected as the name includes raingreen as a classification. But it seems like changes in tree types are dependent on changes in precipitation, while changes in grass types are dependent on temperature in the Sahel Zone.
All in all there have to be more driving factors for the regional changes, as only a part of the vegetation changes can be explained by changes in air surface temperature and precipitation. Mostly in the Siberian region, in difference to the Sahel Zone, the base for growth is more complicated as none of those PFT is dependent on precipitation and only the tree types and the GC3 responds to increasing temperatures.

6 Summary and discussion

In this work by using simple analysis techniques it is shown that the modelled results differ depending on the experiment as expected. It was only taken a look on a selection of CO_2 concentration and orography/ice sheet adaptations present in the PlioMIP2 simulation ensemble, but the main setting of the Eoi^{400} experiment produces similar results to different analyses made before.
The global temperature increase of 3.3°C with local maxima of over 25°C, agree to the description of the Pliocene warm world environment by Salzmann et al. (2011) and Haywood et al. (2013) as well as to Stepanek and Lohmann (2012) in the PlioMIP Phase1. The changes in net-precipitation (Figure 5.6 (a)) are not all compatible with some earlier findings by Haywood et al. (2002) who simulates the atmosphere with the HadAM3. In fact the results mostly agree on the continent's land surface with an increase in Northern Europe, Eastern Russia and Eastern Greenland as well as a decrease in Eastern North America and Eastern China. The net-precipitation shows higher values over Antarctica in both models.
The changes in vegetation types (Figure 5.10) give altogether a good overview of the Mid-Pliocene vegetation distribution with most simulation results agreeing to findings by others. Lunt et al. (2012) concluded a change from ice sheet to boreal forest on Greenland, which is compatible with our results with the addition of grass types in the region of which Lunt et al. (2012) does not speak. The change from desert to grass on the Arabian Peninsula is also consistent. Following Salzmann et al. (2011) the evergreen rain forest belt is said to have almost the same latitudinal position in simulation Eoi^{400} which is in line with results presented here even though the proportion of forest types decreases. The paper also states a retraction of subtropical - and semi-deserts which is compatible with the results for Sahel in Africa where there is in parts a spread of grass and a northward shift of forest and grass types. The most significant change in vegetation distribution in a mid-Pliocene warm world is, and that is compatible with the majority of previous publications (e.g. Haywood et al. (2009); Salzmann et al. (2011)), a northward shift of taiga on the Northern Hemisphere, which is here represented as part of the forest type, in expence of tundra, which is here represented as part of the grass type. Removing the ice sheet on West Antarctica leads to a growth of grass types of almost 100%, being in accordance with Haywood et al. (2002) who report an occurence of lichen moss on Antartica. In addition, Haywood et al. (2009) states a spread of forest in Europe, with which the results in this thesis are not consistent since the JSBACH model produces an increase of grass types on this continent.
Having a clear northward shift of the forest-tundra boundary, it is not surprising that

these results are compatible with the findings of Haywood et al. (2002), showing a high-latitude expansion of forest, Haywood et al. (2009), pointing out a northward displacement of the boreal forest zone, and Salzmann et al. (2011), demonstrating a northward shift of the boundary between tundra and taiga between 250 km in Siberia and 2500 km in the Canadian Arctic. The biggest difference hereby is the amplitude of expansion with about 800 km in Siberia and about 2200 km on Greenland in this work which may be caused by the land-sea-mask as both forest types reach the continent's geographically possible northward placement.
The correlation of the two selected regions in Siberia and Northern Africa are weak for precipitation and vegetation even though they show significant results. It is not very meaningful since there are too few data points to analyse leading to high errors. With a small number of values correlations are more likely to appear even though in reality they may not exist. The limitation also led to the non-usage of the first thought Pearson correlation, preferably thought because it also includes the distribution of the values. All in all the correlation assumes an independence of the variables, which is surely not given in an atmosphere, and is therefore only an approximation. Following the simple axiom of correlation not implying causation (e.g. Holland (1986)) the correlation results are an insight in both regional changes, but do not necessarily prove a change of vegetation due to changes in precipitation and temperature.
As seen in Chapter 5.1 there is only a quasi-equilibrium state. The longer the experiment and computing time the better the results may be as the state of equilibrium of every part of the model increases with the time, mostly because the ocean's quasi-equilibrium state is not reached yet. Another cause of errors is the usage of a time mean, mostly a year mean although it is a 100-year mean. There is a variance of the year as seen e.g. in the correlations of the year mean (see chapter 5.4) and the seasonal mean. That does not only include the differences in temperature and precipitation but also in radiation which was not evaluated in this work and is the engine for many driving factors of the climate. The changes in temperature are due to changes in radiation, more specific in the imbalance of emitted terrestrial and incoming solar radiation. The global mean of the last 100 modeled years of imbalance of Eoi^{400} is 131.62 $\frac{W}{m^2}$ while the E^{280} experiment's energy imbalance is 124.59 $\frac{W}{m^2}$. It can therefore be concluded that on a global mean there is more energy due to more shortwave radiation or less longwave radiation on the surface for the Pliocene, since the solar constant is equal for the experiments. A higher CO_2 concentration leads to a positive imbalance at top of the atmosphere, which heats the Earth (Mauritsen et al. (2013)). Therefore a correlation and causation is evident, but its appearance and strength is not researched here.

7 Outlook

With the members of the PlioMIP Phase 2 working on analysing the modelled results and establishing (sensitivity) studies some of the next points may already be in work to further describe and improve the Mid-Pliocene warm climate.
With this thesis only giving a small insight into the experiments the focus may not only be on the main core experiment Eoi^{400}. Furthermore a focus on the climate anomalies caused by higher CO_2 would give a deeper insight into the model as well as the future, since the CO_2 concentration is currently still rising. The changes of vegetation types grass and forest in dependence of the CO_2 concentration for pre-Industrial and Pliocene orography and ice sheet configuration for the regions of Siberia and Africa can be found in the appendix. Also the study of other regions with high changes, like the Amazonian rain forest, the European continent and Greenland or regions with less changes like Australia and Southern Russia can be of interest. Especially a comparison of the conditions in regions with high and low changes can give important informations on the evolution of vegetation. AThis thesis focuses on the atmosphere and vegetation changes, but also the ocean plays an important role and should be taken into account or further analyses since all three climate system components act jointly. This also adds new variables for analysis. The influence of temperature and precipitation on biomes is clear but also light/shadow as well as soil properties have a huge influence on the growth of plants. Especially a dynamic soil module in the model may help to improve vegetation dynamics beyond the current restriction by the model implementation. The landcover library concentrates, e.g., on chemical rates which include carbon content that is directly influenced by rising CO_2 concentration, albedos, and temperature ranges. That offers a variety of other variables to take into account to show a correlation of atmosphere to lithosphere and biosphere. While the biosphere in JSBACH consists of 8 PFT the results could be more precise with an implementation of more specific plant types and not only plant functional types, like the BIOME4 model, which resolves a 28 biome classification (Salzmann et al. (2008)). On the other hand this leads to more complications and a higher data quantity and computing time as well as maybe an easier analogy from modern to Mid-Pliocene vegetation types or a difficult analogy as they are not consistent.

List of Figures

Bibliography

Beck, E.-G. (2008). 50 Years of Continuous Measurement of CO 2 on Mauna Loa. *Energy & Environment*, 19:1017–1028.

Chandan, D. and Peltier, W. R. (2017). Regional and global climate for the mid-pliocene using the university of toronto version of ccsm4 and pliomip2 boundary conditions. *Climate of the Past*, 13(7):919–942.

Chandan, D. and Peltier, W. R. (2018). On the mechanisms of warming the mid-pliocene and the inference of a hierarchy of climate sensitivities with relevance to the understanding of climate futures. *Climate of the Past*, 14(6):825–856.

Chandler, M. A., editor (1997). *The Climate of the Pliocene: Simulating Earth's Last Great Warm Period*.

Dowsett, H. J., Dolan, A. M., Rowley, D., Moucha, R., Forte, A., Mitrovica, J. X., Pound, M., Salzmann, U., Robinson, M. M., Chandler, M., Foley, K. M., and Haywood, A. M. (2016). The PRISM4 (mid-Piacenzian) paleoenvironmental reconstruction. *Climate of the Past*, 12(7):1519–1538.

Dowsett, H. J., Haywood, A. M., Valdes, P. J., Robinson, M. M., Lunt, D. J., Hill, D. J., Stoll, D. K., and Foley, K. M. (2011). Sea surface temperatures of the mid-Piacenzian Warm Period: A comparison of PRISM3 and HadCM3. *Palaeogeography, Palaeoclimatology, Palaeoecology*, 309(1):83 – 91. Special Issue: Climate and seasonality in a Pliocene warm world.

Epp, L. S., Kruse, S., Kath, N. J., Stoof-Leichsenring, K. R., Tiedemann, R., Pestryakova, L. A., and Herzschuh, U. (2018). Temporal and spatial patterns of mitochondrial haplotype and species distributions in Siberian larches inferred from ancient environmental DNA and modeling. *Scientific Reports*, 8(1):17436.

Haywood, A. M., Chandler, M. A., Valdes, P. J., Salzmann, U., Lunt, D. J., and Dowsett, H. J. (2009). Comparison of mid-Pliocene climate predictions produced by the HadAM3 and GCMAM3 General Circulation Models. *Global and Planetary Change*, 66(3):208 – 224.

Haywood, A. M., Dowsett, H. J., Dolan, A. M., Rowley, D., Abe-Ouchi, A., Otto-Bliesner, B., Chandler, M. A., Hunter, S. J., Lunt, D. J., Pound, M., and Salzmann, U. (2016). The Pliocene Model Intercomparison Project (PlioMIP) Phase 2: Scientific objectives and experimental design. *Climate of the Past*, 12(3):663–675.

Haywood, A. M., Dowsett, H. J., Robinson, M. M., Stoll, D. K., Dolan, A. M., Lunt, D. J., Otto-Bliesner, B., and Chandler, M. A. (2011). Pliocene Model Intercomparison Project (PlioMIP): experimental design and boundary conditions (Experiment 2). *Geoscientific Model Development*, 4:571–577.

Haywood, A. M., Hill, D. J., Dolan, A. M., Otto-Bliesner, B. L., Bragg, F., Chan, W.-L., Chandler, M. A., Contoux, C., Dowsett, H. J., Jost, A., Kamae, Y., Lohmann, G., Lunt, D. J., Abe-Ouchi, A., Pickering, S. J., Ramstein, G., Rosenbloom, N. A., Salzmann, U., Sohl, L., Stepanek, C., Ueda, H., Yan, Q., and Zhang, Z. (2013). Large-scale features of Pliocene climate: results from the Pliocene Model Intercomparison Project. *Climate of the Past*, 9:191–209.

Haywood, A. M., Valdes, P. J., Francis, J. E., and Sellwood, B. W. (2002). Global middle Pliocene biome reconstruction: A data/model synthesis. *Geochemistry, Geophysics, Geosystems*, 3(12):1–18.

Hill, D. J., Haywood, A. M., Lunt, D. J., Hunter, S. J., Bragg, F. J., Contoux, C., Stepanek, C., Sohl, L., Rosenbloom, N. A., Chan, W.-L., Kamae, Y., Zhang, Z., Abe-Ouchi, A., Chandler, M. A., Jost, A., Lohmann, G., Otto-Bliesner, B. L., Ramstein, G., and Ueda, H. (2014). Evaluating the dominant components of warming in Pliocene climate simulations. *Climate of the Past*, 10:79–90.

Holland, P. W. (1986). Statistics and Causal Inference. *Journal of the American Statistical Association*, 81(396):945–960.

Kamae, Y., Yoshida, K., and Ueda, H. (2016). Sensitivity of Pliocene climate simulations in MRI-CGCM2.3 to respective boundary conditions. *Climate of the Past*, 12(8):1619–1634.

Liu, Z., Notaro, M., Kutzbach, J., and Liu, N. (2006). Assessing Global VegetationClimate Feedbacks from Observations. *Journal of Climate*, 19(5):787–814.

Lohmann, G., Butzin, M., and Bickert, T. (2015). Effect of Vegetation on the Late Miocene Ocean Circulation. *Journal of Marine Science and Engineering*, 3(4):1311–1333.

Lunt, D. J., Haywood, A. M., Schmidt, G. A., Salzmann, U., Valdes, P. J., Dowsett, H. J., and Loptson, C. A. (2012). On the causes of mid-Pliocene warmth and polar amplification. *Earth and Planetary Science Letters*, 321-322:128 – 138.

Mauritsen, T., Graversen, R. G., Klocke, D., Langen, P. L., Stevens, B., and Tomassini, L. (2013). Climate feedback efficiency and synergy. *Climate Dynamics*, 41(9):2539–2554.

Pagani, M., Liu, Z., LaRiviere, J., and Ravelo, A. C. (2009). High Earth-system climate sensitivity determined from Pliocene carbon dioxide concentrations. *Nature Geoscience*, 3:27.

Prentice, I. C., Cramer, W., Harrison, S. P., Leemans, R., Monserud, R. A., and Solomon, A. M. (1992). A global biome model based on plant physiology and dominance, soil properties and climate. *Journal of Biogeography*, 19(2):117–134.

Raddatz, T., H. Reick, C., Knorr, W., Kattge, J., Roeckner, E., Schnur, R., Schnitzler, K.-G., Wetzel, P., and Jungclaus, J. (2007). Will the tropical land biosphere dominate the climatecarbon cycle feedback during the twenty-first century? *Climate Dynamics*, 29:565–574.

Reick, C. H., Raddatz, T., Brovkin, V., and Gayler, V. (2013). Representation of natural and anthropogenic land cover change in MPI-ESM. *Journal of Advances in Modeling Earth Systems*, 5(3):459–482.

Salzmann, U., Haywood, A., and Lunt, D. (2009). The past is a guide to the future? Comparing Middle Pliocene vegetation with predicted biome distributions for the twenty-first century. *Philosophical Transactions of the Royal Society A: Mathematical, Physical and Engineering Sciences*, 367(1886):189–204.

Salzmann, U., Haywood, A. M., Lunt, D. J., Valdes, P. J., and Hill, D. J. (2008). A new global biome reconstruction and data-model comparison for the Middle Pliocene. *Global Ecology and Biogeography*, 17(3):432–447.

Salzmann, U., Williams, M., Haywood, A. M., Johnson, A. L., Kender, S., and Zalasiewicz, J. (2011). Climate and environment of a Pliocene warm world. *Palaeogeography, Palaeoclimatology, Palaeoecology*, 309(1):1 – 8. Special Issue: Climate and seasonality in a Pliocene warm world.

Schoenwiese, C.-D. (1985). *Praktische Statistik fuer Meteorologen und Geowissenschaftler*. Gebrueder Borntraeger, Berlin . Stuttgart.

Stepanek, C. and Lohmann, G. (2012). Modelling mid-Pliocene climate with COSMOS. *Geoscience Model Dev.*, 5:1221–1243.

Storch, H. and Zwiers, F. (1999). *Statistical Analysis in Climate Research*. Cambridge University Press.

Walter, H. (1973). *Vegetation of the earth in relation to climate and the eco-physiological conditions*. English Universities Press.

Zheng, J., Zhang, Q., Li, Q., Zhang, Q., and Cai, M. (2019). Contribution of sea ice albedo and insulation effects to Arctic amplification in the EC-Earth Pliocene simulation. *Climate of the Past*, 15(1):291–305.

Appendix

regional influence of CO_2 concentration on grass and forest types

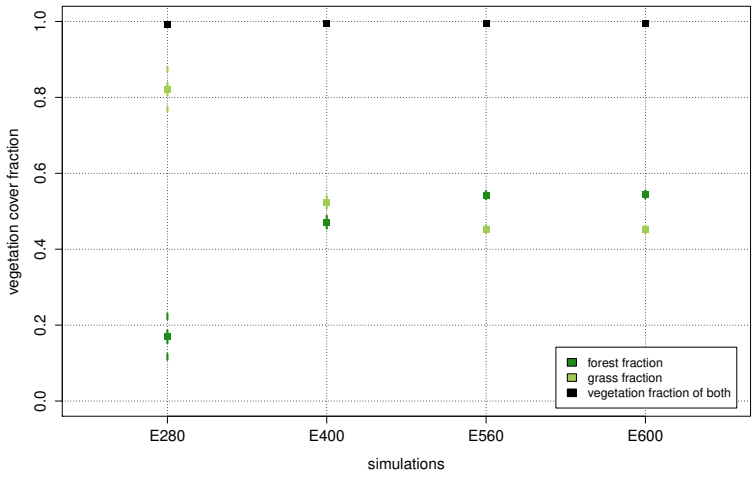

(a)

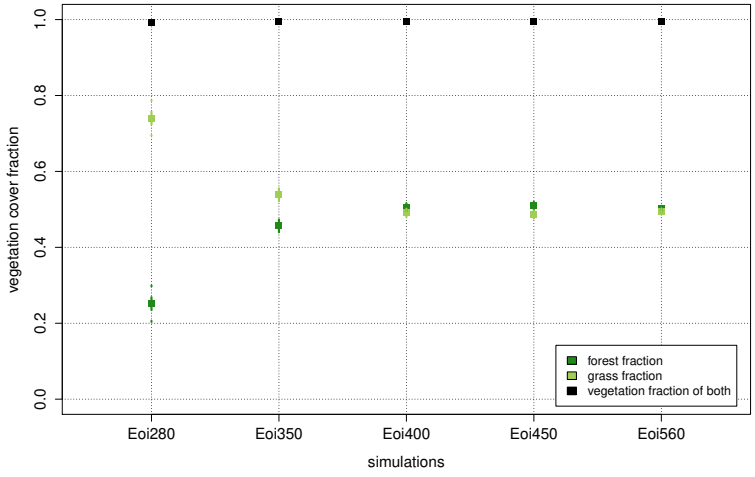

(b)

Figure A1: Changes in plant cover divided into grass and forest (see Chapter 3.2.2) for (a) solely modern day geography with rising CO_2 concentration and (b) with Mid-Pliocene configurations and rising CO_2 concentration. The plant cover fraction average over the Siberian region shown in Figure 5.13 is hereby plotted with the variances. These variances are variations in areas cover fraction appearances and insignificantly small for most simulations.

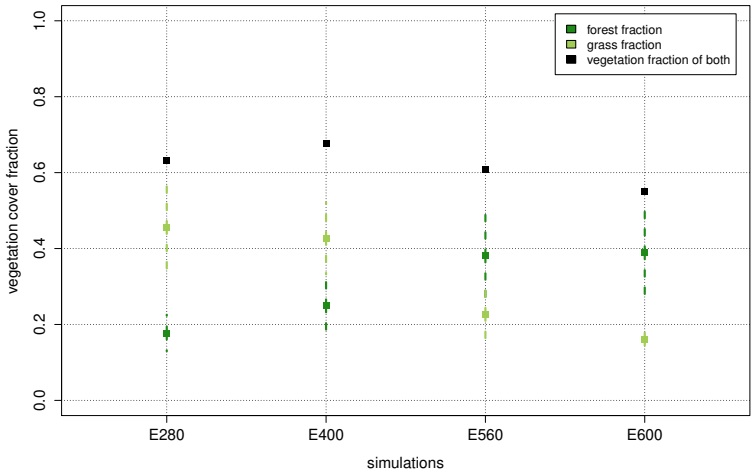

(a)

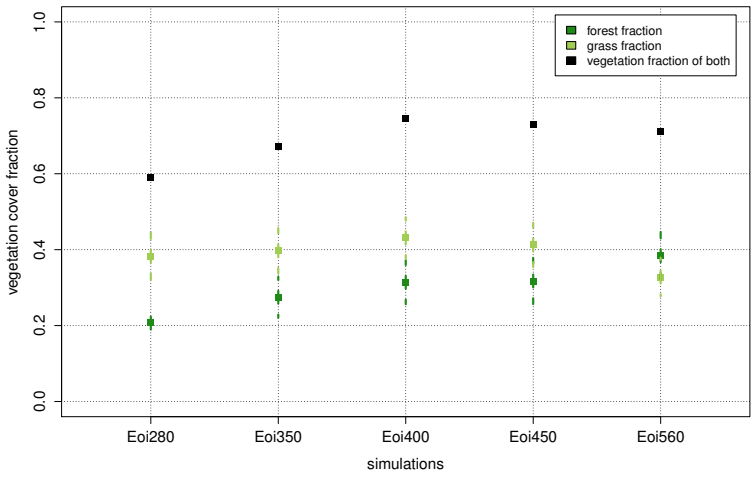

(b)

Figure A2: Changes in plant cover divided into grass and forest (see Chapter 3.2.2) for (a) solely modern day geography with rising CO_2 concentration and (b) with Mid-Pliocene configurations and rising CO_2 concentration. The plant cover fraction average over the African Sahel region shown in Figure 5.13 is hereby plotted with the variances. These variances are variations in areas cover fraction appearances and insignificantly small for most simulations.

factorization

Within the framework of PlioMIP2 various sensitivity studies have been run not only the four used in this thesis. To get a restriction to some main experiments the experiments with the most influence on atmospheric changes were chosen. With the use of the

factorization given by Haywood et al. (2016), the impact of each boundary condition ice sheet, orography and CO_2 concentration on the overall Pliocene climate can be calculated as follows:

$$\Delta T = dT_{CO_2} + dT_{oro} + dT_{ice} \tag{A1}$$

with

$$dT_{CO_2} = \frac{1}{4}((E^{400} - E^{280}) + (Eo^{400} - Eo^{280}) + (Ei^{400} - Ei^{280}) + (Eoi^{400} - Eoi^{280})) \tag{A2}$$

$$dT_{oro} = \frac{1}{4}((Eo^{280} - E^{280}) + (Eo^{400} - E^{400}) + (Eoi^{280} - Ei^{280}) + (Eoi^{400} - Ei^{400})) \tag{A3}$$

$$dT_{ice} = \frac{1}{4}((Ei^{280} - E^{280}) + (Ei^{400} - E^{400}) + (Eoi^{280} - Eo^{280}) + (Eoi^{400} - Eo^{400})) \tag{A4}$$

By using these equations as well as a 100-year- and global surface air temperature average, results of the warming contribution have been calculated (see Table A1).

	quantity in °C	percentage of ΔT
dT_{CO_2}	2.23	67.31%
dT_{oro}	0.91	27.32%
dT_{ice}	0.18	5.37%

Table A1: The warming contribution of each model boundary condition of E-, Eo-, Ei-, $Eoi^{280/400}$ using equation A2 for dT_{CO_2}, equation A3 for dT_{oro} and equation A4 for dT_{ice}.

The table A1 shows that there is a contribution to warming in the Pliocene of about $\frac{2}{3}$ by the CO_2, whereas orography and ice sheet changes combined only take up about $\frac{1}{3}$. While the focus remains on the impact of CO_2, analyses of the results are carried out with the model output by orography and ice sheet combined. That is why the four experiments of Table 3.1 (E^{280}, E^{400}, Eoi^{280} and Eoi^{400}) are used..

Ehrenwörtliche Erklärung

Hiermit erkläre ich, dass ich die vorliegende Bachelorarbeit selbstständig angefertigt habe; die aus fremden Quellen direkt oder indirekt übernommenen Gedanken sind als solche kenntlich gemacht. Die Bachelorarbeit habe ich bisher keinem anderen Prüfungsamt in gleicher oder vergleichbarer Form vorgelegt. Sie wurde bisher auch nicht veröffentlicht.

Ort, Datum Unterschrift